ACS Photonics

pubs.acs.org/journal/apchd5
Review

Designing Metasurfaces for Efficient Solar Energy Conversion

Published as part of ACS Photonics virtual special issue "Photonics for Energy".

Luca Mascaretti, Yuheng Chen, Olivier Henrotte, Omer Yesilyurt, Vladimir M. Shalaev, Alberto Naldoni,* and Alexandra Boltasseva*

Cite This: https://doi.org/10.1021/acsphotonics.3c01013

ABSTRACT: Metasurfaces have recently emerged as a promising technological platform, offering unprecedented control over light by structuring materials at the nanoscale using two-dimensional arrays of subwavelength nanoresonators. These metasurfaces possess exceptional optical properties, enabling a wide variety of applications in imaging, sensing, telecommunication, and energy-related fields. One significant advantage of metasurfaces lies in their ability to manipulate the optical spectrum by precisely engineering the geometry and material composition of the nanoresonators' array. Consequently, they hold tremendous potential for efficient solar light harvesting and conversion. In this Review, we delve into the current state-of-the-art in solar energy conversion devices based on metasurfaces. First, we provide an overview of the fundamental processes involved in solar energy conversion, alongside an introduction to the primary classes of metasurfaces, namely, plasmonic and dielectric metasurfaces. Subsequently, we explore the numerical tools used that guide the design of metasurfaces, focusing particularly on inverse design methods that facilitate an optimized optical response. To showcase the practical applications of metasurfaces, we present selected examples across various domains such as photovoltaics, photoelectrochemistry, photocatalysis, solar-thermal and photothermal routes, and radiative cooling. These examples highlight the ways in which metasurfaces can be leveraged to harness solar energy effectively. By tailoring the optical properties of metasurfaces, significant advancements can be expected in solar energy harvesting technologies, offering new practical solutions to support an emerging sustainable society.

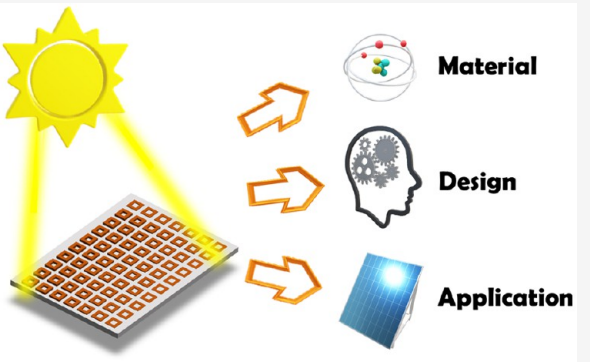

KEYWORDS: *metasurfaces, plasmonics, dielectric, solar energy conversion, inverse design, optical response*

1. INTRODUCTION

Our current energy system is facing an unprecedented challenge in transitioning from the current fragile and unsustainable model, which has led to global warming and is affected by price volatility and shortfalls in the supply, toward a fair, resilient, and sustainable one.[1] Such an ambitious goal has been set by international negotiations, such as the so-called Paris Agreement,[2] which has set a net carbon neutrality target by 2050. This implies massive efforts in developing a wide range of energy conversion solutions, both centralized and decentralized, not only to make use of all the potential natural resources but also to mitigate the risk of supply disruption. A similar concept applies to the sources of raw materials to produce such devices, which should be as diverse as possible and should focus on Earth-abundant materials. As a clean source of energy to mitigate the current worrying energy crisis, sunlight is particularly desirable because it is decentralized, practically inexhaustible, and copious. Indeed, it accounts for ∼120000 TW of daily power reaching the Earth's surface,[3] thus euphemistically outdistancing today's global average power consumption of ∼20 TW.[4] Only a tiny fraction of solar energy is practically used today, though, mainly through photovoltaic and solar-thermal technologies, while other approaches, including photocatalysis, are confined at the laboratory scale, despite decades of research. Scientists are therefore ceaselessly devising new solutions to better exploit solar energy to generate electricity, heat, and chemicals.

Metasurfaces (see refs 5−26 for historical and comprehensive reviews and references therein) have recently emerged as a promising platform to harvest and transform sunlight. They can be defined as two-dimensional (2D) arrays of nanoantennas (also termed nanoresonators or meta-atoms) with subwavelength dimensions[5−26] that exhibit a wide range of properties imparted by their peculiar design which, otherwise, would be unachievable in bulk materials. After early demonstrations of

Received: July 18, 2023
Revised: November 1, 2023
Accepted: November 1, 2023

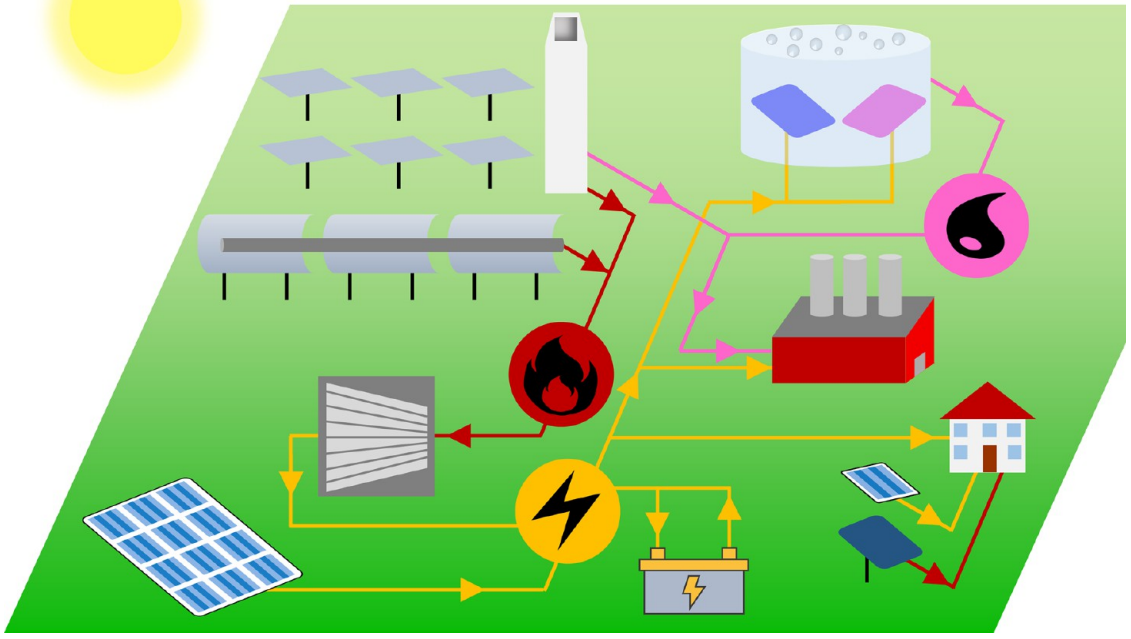

Figure 1. Schematic overview of solar energy conversion processes that lead to electricity (thunderbolt symbol), heat (flame symbol), or fuel (drop symbol) generation.

unusual optical effects,[27−29] the extreme light manipulation capability of metasurfaces has led to a wide variety of applications.[10,12,30,31] These materials may thus play an initially unforeseen role in solar energy conversion thanks to their high optical tunability.[32−35] Furthermore, metasurfaces can be readily synthesized by low-cost and scalable fabrication processes, such as photolithography, which is compatible with the semiconductor microelectronic industry.[36]

This Review focuses on solar energy conversion concepts utilizing metasurfaces. We first discuss the fundamental aspects of solar energy conversion (section 2) and the main physical processes occurring in materials upon light absorption in two main classes of metasurfaces, i.e., plasmonic and dielectric (section 3). As highlighted by the increasingly important role of inverse design and numerical simulations in various scientific fields, the role of such tools in the design of metasurfaces tailored to specific solar energy conversion routes is presented (section 4). Afterward, selected examples of metasurface applications in photovoltaics, photo(electro)catalysis, and solar-thermal routes are discussed (section 5). To conclude, the potential of practical metasurfaces and targeted applications is summarized, together with the critical factors to be addressed for large-scale implementation, benchmarking, and further exploration of unusual optical effects (section 6). We note that this review does not present an extensive discussion on the physics, fabrication, and general applications of metasurfaces, which are available elsewhere.[5,14,18,23,37] This Review focuses on the essential physical mechanisms of solar energy conversion and resonant phenomena in metasurfaces by examining selected experimental results and discussing advanced design methods. The latter, especially machine learning and inverse design algorithms,[8,38−41] play an increasingly important role in the realization of efficient metasurfaces for light harvesting and conversion. By considering metasurface concepts for solar energy conversion and design tools enabled by advanced computational methods, this work may foster further efforts toward the practical implementation of metasurfaces for renewable energy technologies.

2. SOLAR ENERGY CONVERSION PROCESSES

Solar light is an abundant source of energy, but it is also intrinsically affected by an intermittent nature. Therefore, the scientific community has devised strategies to both harvest and either directly utilize or store it for later use. An overview of such technologies (Figure 1) is briefly discussed below, highlighting the potential of metasurfaces in each of these energy conversion processes.

Photovoltaic (PV) technology allows the direct conversion of solar energy into electricity and is the most mature among all solar energy conversion processes (see refs 42−44 and references therein). The main component of a PV cell is a semiconductor material that generates charge carriers (electron−hole pairs) upon light absorption with energy greater than its bandgap (E_g). Typical materials are low-band gap semiconductors, mainly silicon (Si, E_g = 1.14 eV), but also cadmium telluride (CdTe) or gallium arsenide (GaAs). The photogenerated carriers need to be separated and reach the surface of the semiconductor to give rise to a photocurrent, which is described by the (minority) carrier diffusion length. Therefore, the material thickness must reach a compromise to achieve sufficient light absorption and limit the recombination rate, which can be addressed by nanostructuring. Typical efficiencies of commercial Si PV cells range from 20 to 25%.[45,46]

Another process that has reached commercial maturity is solar-thermal conversion.[47] The representative device is a solar thermal collector (or receiver), which in turn is in contact with a fluid (heat transfer fluid, HTF) that is either directly utilized for heating or to generate electricity. The first scenario is typical of low-temperature devices (~100 °C) that are used to heat up water or air and are available for decentralized industrial or

https://doi.org/10.1021/acsphotonics.3c01013
ACS Photonics XXXX, XXX, XXX−XXX

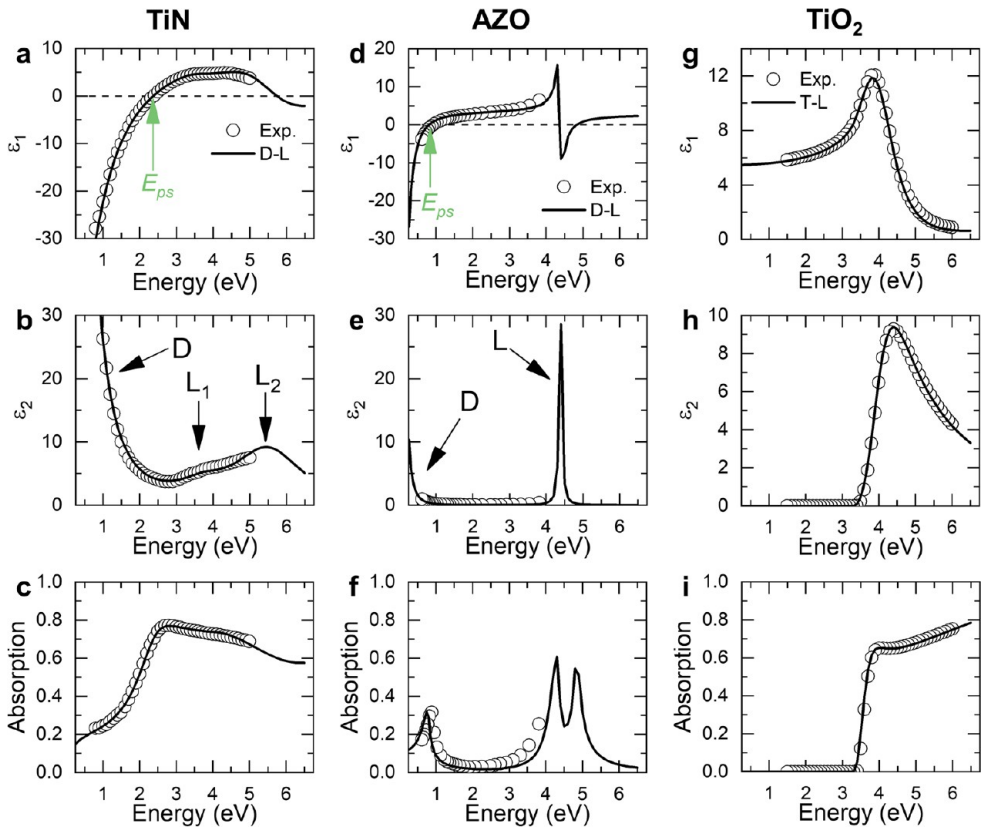

Figure 2. Examples of relevant materials for solar energy conversion applications selected by the authors (modeled with Drude−Lorentz and Tauc−Lorentz oscillators). In all cases, absorptance spectra were computed using the formulas from ref 77 for 100 nm thick free-standing films. (a−c) Titanium nitride (TiN, experimental data, and modeling with one Drude and two Lorentz oscillators from ref 78). (d−f) Aluminum-doped zinc oxide (AZO, 2 wt % Al, experimental data, and modeling with one Drude and one Lorentz oscillator from ref 79). (g−i) Titanium dioxide (TiO_2, experimental data from ref 80 and modeled with a Tauc−Lorentz oscillator).

domestic use thanks to their limited cost. The second scenario is known as concentrating solar power (CSP) or thermodynamic solar power and makes use of complex optical systems (such as solar fields) to concentrate light up to concentrating factors ∼1000 heating the HTF up to ∼1000 °C. This is necessary to increase the efficiency of electricity generation by a steam engine. Alternative solar-thermal strategies beyond the two aforementioned ones are, for example, solar ponds and solar distillation or desalination, which are potentially interesting for remote locations.[48] Unlike the case of PV, solar-thermal processes do not involve any excitation and transport of charge carriers, but rather heat generation upon photon absorption and subsequent dissipation of the light energy into lattice phonons. Therefore, metallic materials can be employed as receivers, because they can reach high temperatures under irradiation. The amount of absorbed light energy can be expressed by the so-called spectrally averaged solar absorptance, $\overline{\alpha}$. However, a hot surface at the temperature T re-emits radiation according to the product $\overline{\varepsilon}\sigma T$,[4] where $\overline{\varepsilon}$ is the spectrally averaged emittance and σ is the Stefan−Boltzmann constant. Radiative heat losses are negligible in low-temperature applications, where convective losses are predominant but must be carefully minimized in CSP applications. An exception to this rule is the case of radiative cooling,[49] which indeed exploits radiative losses to cool down a hot surface even during daytime. This is not a solar energy conversion technology by itself but is an approach with high potential to improve the energy efficiency of devices and buildings. All such solar-thermal routes require a careful design of the solar absorber material and of its absorption spectrum, thus achieving a spectrally selective behavior and further a selection of appropriate materials withstanding repeated and severe thermal cycling.

Sunlight can be further employed to generate chemicals and fuels, therefore being stored and circumventing its intrinsic intermittent nature. In the case of photocatalysis, semiconductor materials generate charge carriers (as in the case of PV) that possess sufficient energy to break chemical bonds of molecules and transform them into fuels, such as splitting water (H_2O) for hydrogen production (H_2).[50−52] Photoelectrochemical (PEC) cells are based on a similar concept, but they involve the use of two separate electrodes, i.e., a (photo)cathode and a (photo)-anode, with the assistance of an external voltage.[53,54] While H_2 can be produced by conventional electrocatalysis (water electrolysis), the same has not been achieved yet by photocatalysis nor by photoelectrochemistry, and typical solar-to-fuel efficiencies are below 10%.[52,55] This is related to a minimum energy threshold required to split the desired molecule and to a relatively inefficient charge transfer at the semiconductor-liquid interface, both of which are absent in PV technology.

An alternative approach to generate fuels using sunlight takes inspiration from the CSP technology according to the thermochemical approach, where no catalytic reaction occurs.[56] Rather, the collector of a CSP plant contains a reducible metal oxide (such as ceria, CeO_2) in contact with the chemical feedstock (such as CO_2 or H_2O), which undergoes two-step

https://doi.org/10.1021/acsphotonics.3c01013
ACS Photonics XXXX, XXX, XXX−XXX

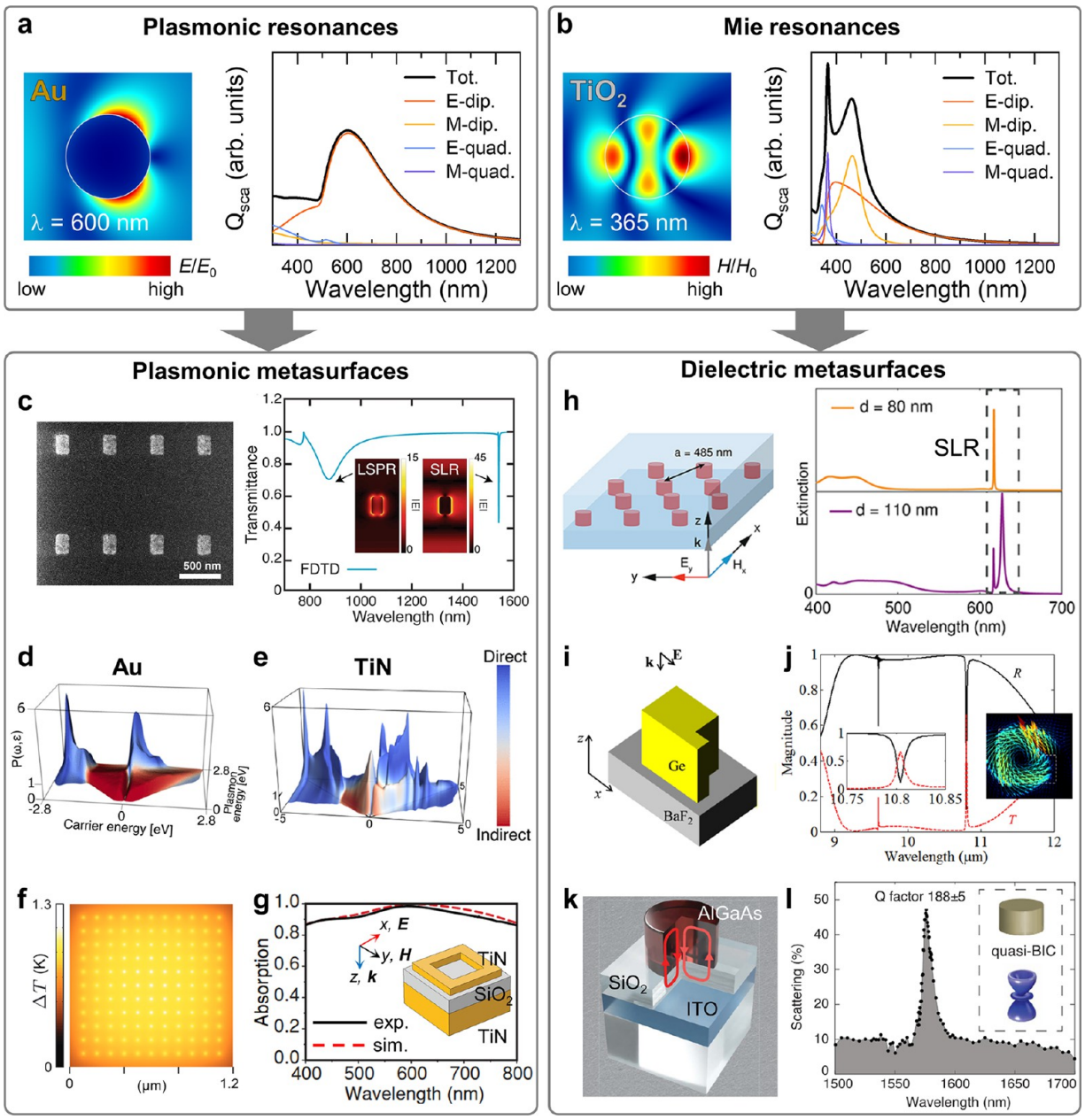

Figure 3. Plasmonic and dielectric metasurfaces. (a) Plasmon resonances for an isolated spherical Au particle (100 nm diameter) in the air/electric field map under excitation wavelength = 600 nm (left) and scattering efficiency (right). (b) Mie resonances for an isolated TiO_2 spherical particle (100 nm diameter) in an air/magnetic field map under an excitation wavelength of 365 nm (left) and scattering efficiency (right). Calculations in (a) and (b) are evaluated by Mie theory using an online calculator[124] and show the electric (E) and magnetic (M) dipolar (dip.) and quadrupolar (quad.) terms. (c) Plasmonic metasurface made of Au rectangular nanostructures exhibiting a sharp SLR (left: electron microscope image; right: finite difference time domain simulations of transmission spectrum under *x*-polarized light; inset: magnitude of the electric field of the LSPR and SLR modes in the *x*-*y* unit cell midplane). Reproduced from ref.[125] Copyright 2021 Author(s), licensed under a CC-BY Creative Commons Attribution 4.0 License. (d) Energy distribution of hot carriers generated by the decay of surface plasmons via intraband (red) or interband (blue) transitions in Au. Adapted with permission from ref 92. Copyright 2016 American Chemical Society. (e) Same as (d), but for TiN. Adapted with permission from ref 93. Copyright 2018 Institute of Physics. (f) Simulated temperature map of a square lattice of 16 nm spherical Au nanoparticles (100 nm periodicity) under a uniform continuous wave laser beam. Adapted with permission from ref 95. Copyright 2013 American Chemical Society. (g) Simulated and measured absorption spectra of a square-array TiN metasurface. Adapted with permission from ref 100. Copyright 2014 Wiley-VCH. (h) Dielectric metasurface made of a hexagonal array of Si nanocylinders with 100 nm height embedded in fused SiO_2 (left) and a corresponding shift of the SLR by changing the diameter of the cylinders (right). Adapted with permission from ref 103. Copyright 2019 Authors, licensed under a CC-BY Creative Commons Attribution 4.0 License. (i) Schematic of the unit cell of broken-symmetry Ge resonators and (j) simulated reflectance (R) and transmittance (T) spectra of the corresponding metasurface with 4.2 μm periodicity (left inset: resonance at ~10.8 μm with Q factor ~1300; right inset: vector plot of the electric field in the $x-y$ resonator midplane). Adapted with permission from ref 110. Copyright 2016 American Chemical Society. (k) Schematic of the unit cell and (l) measured scattering spectrum of a dielectric metasurface made of AlGaAs disk resonators supporting quasi-bound states in the continuum (quasi-BICs, as shown by the electric field pattern in the inset). Adapted with permission from ref 114. Copyright 2020 American Association for the Advancement of Science.

https://doi.org/10.1021/acsphotonics.3c01013
ACS Photonics XXXX, XXX, XXX−XXX

reversible redox cycles and allows producing the desired fuels (such as CO or H_2).

The essential features of the aforementioned technologies can also be combined with hybrid approaches. For example, thermophotovoltaics (TPV) is based on the absorption of sunlight by a selective absorber-emitter structure and by its subsequent thermal emission that matches the bandgap of an adjacent PV cell.[57,58] This strategy is attractive in terms of its high spectral management, because the absorber unit can fully utilize the solar spectrum and sub-band gap photons can be reflected from the PV cell to the emitter and, subsequently, reabsorbed. However, it requires refractory materials withstanding temperatures as high as ∼2000 °C. Furthermore, the combination of photocatalytic and photothermal processes has recently emerged in the scientific literature under the nomenclature of photothermal catalysis.[59] This route aims at synergistically combining electronic and thermally driven catalytic effects to drive either exothermic or endothermic reactions relevant to the chemical industry without the need for extreme concentration regimes of CSP.

In all of these scenarios, metasurfaces can offer critical advantages to improve the performance of solar energy conversion devices.[32,60] For example, the metasurface absorption spectrum can be tailored by engineering optical resonant modes ruled by the geometry and constituent materials. Thus, it is possible to increase both the optical absorption of PV/PEC cells and broadband optical absorption for low-temperature solar-thermal conversion or, conversely, to achieve a high spectral selectivity for high-temperature applications as well as to induce a narrow absorption peak in the mid-IR (MIR) for thermal emitters for radiative cooling. Electric field enhancement effects arising in metasurfaces can be further engineered to increase the photogeneration rate in semiconductor materials and lead to hot carrier injection to the photoactive unit, which can boost the performance of PV, photocatalysis, and photoelectrochemistry processes. Moreover, metasurfaces consisting of refractory metals and insulators can exhibit nearly perfect optical absorption within a subμm thickness,[61−63] therefore reaching high temperatures under moderate light concentrations (∼20), therefore dramatically increasing the receiver efficiency in solar-thermal applications.

3. MATERIALS FOR METASURFACES

3.1. Introduction to Optical Materials for Energy-Related Applications. The dielectric function (or permittivity) that governs the light−matter interaction is the central parameter to consider when designing efficient optical devices. Figure 2 illustrates selected examples of dielectric permittivities and absorption spectra of relevant materials for solar energy conversion processes that we chose to discuss. The first is titanium nitride (TiN), an emerging plasmonic material alternative to gold (Au)[64−72] that belongs to a class of transition metal nitrides (TMNs). TMNs represent a promising platform for energy-related applications due to their robustness, high-temperature stability, low cost, and versatility.[73] TiN exhibits a large negative ε_1 (Figure 2a) and a large positive ε_2 (Figure 2b) in the low-energy region, in turn, associated with high reflectance and relatively low absorptance (Figure 2c). Thus, in the energy region where $\varepsilon_1 < 0$, the material exhibits plasmonic resonances. By increasing the energy, ε_1 switches signs at the so-called crossover wavelength (λ_{ps}) or screened plasma energy ($E_{ps} \sim 2.4$ eV in Figure 2a) and the absorptance reaches a maximum (Figure 2c). In the region $\varepsilon_1 > 0$, interband transitions take place, which are responsible for a high optical absorption and can be represented with the Lorentz model (for TiN, two Lorentz oscillators are indicated in Figure 2b). Finally, another region of metallic behavior occurs at high energies, but it is less important in terms of solar energy conversion applications being beyond the onset of the solar spectrum onset. The second selected material is aluminum-doped zinc oxide (AZO), an Earth-abundant transparent conducting oxide (TCO) for solar cells (see ref 74 and references therein). This material exhibits metallic behavior in the low energy region, i.e., $\varepsilon_1 < 0$ for energies $E < E_{ps}$, and the crossover wavelength in the near-IR (NIR) range ($E_{ps} \sim 0.8$ eV in Figure 2d). It is characterized by a high transparency region in the visible range (Figure 2e) and negligible absorptance (Figure 2f) in the range 1−3 eV. This is a typical feature of TCOs, which generally exhibit a wide bandgap ($E_g > 3$ eV). The Drude−Lorentz model, however, does not represent the actual physical bandgap of semiconductors or insulators and indeed does not satisfactorily reproduce the high absorption upon bandgap transitions ($E_g \sim 3.5$ eV in Figure 2f). The third material, titanium dioxide (TiO_2), is a typical wide-bandgap oxide photocatalyst (see refs 75 and 76 and references therein). Its optical behavior can be reproduced by the so-called Tauc−Lorentz model, which explicitly incorporates the bandgap into its expression. Due to its poorly conductive nature, ε_1 in TiO_2 is always positive (Figure 2g), while ε_2 is zero in a wide energy range up to the ultraviolet region of the electromagnetic spectrum where bandgap transitions occur ($E_g \sim 3.3$ eV in Figure 2h). Therefore, no intraband absorption occurs in undoped TiO_2, but only interband absorption occurs for energies higher than E_g (Figure 2i). These three exemplary materials exhibit different optical behavior and are employed to produce metasurfaces operating in different spectral regions.

3.2. Plasmonic and Dielectric Metasurfaces. The optical behavior of individual resonators that are employed to design metasurfaces can be generally explained in terms of multipole resonances.[81,82] However, while the optical spectrum of metallic nanoparticles is dominated by the electric dipole term, representing the so-called localized surface plasmon resonance (LSPR, Figure 3a),[83] dielectric nanoparticles show the features of the magnetic dipole and quadrupole terms, or Mie resonances (see the example for a TiO_2 sphere with $2R = 100$ nm, Figure 3b). Plasmonic metasurfaces are obtained by arranging nanoscale metallic resonators into an array (Figure 3c), and their optical response can be engineered by the geometry of the structure. For example, the so-called surface lattice resonance (SLR) occurs when the periodicity is comparable to the incident light wavelength.[84] The SLR exhibits a high quality factor (or Q-factor), defined as the ratio between the resonance wavelength and its width, i.e., $Q = \lambda_{min}/\Delta\lambda$, and it is usually narrower than the LSPR of the individual resonators (Figure 3c). Therefore, by means of SLRs, plasmonic metasurfaces offer high electric field enhancement and, in turn, higher charge carriers' generation in a nearby photoactive material (see section 5). Plasmonic metasurfaces also enhance the energetic "hot" carriers generation upon plasmon excitation and decay,[85,86] which is relevant for PV cells[87] and photocatalysis.[88−91] For example, plasmon decay in Au is strongly affected by interband transitions, which leads to an asymmetric energy distribution of charge carriers (Figure 3d),[92] while the carrier distribution in TiN is more complex due to a more complicated band structure (Figure 3e).[93] Such theoretical results are crucial to assess the suitability of metasurfaces based on plasmonic metals combined with n- or p-type semiconductors and for reductive or oxidative

https://doi.org/10.1021/acsphotonics.3c01013
ACS Photonics XXXX, XXX, XXX−XXX

photochemical reactions. Excited charge carriers eventually thermalize (if not extracted to generate a photocurrent or to drive chemical reactions) and dissipate their energy toward the environment. In particular, the density of heat produced upon photon absorption is proportional to $\sim\varepsilon_2(\omega)|\mathbf{E}(\mathbf{r})|^2$, where $\mathbf{E}(\mathbf{r})$ is the electric field distribution inside the material.[94] As a consequence, metals with large values of $\varepsilon_2(\omega)$ are suitable to generate photothermal effects (Figure 2b,e), unlike semiconductors and insulators due to the negligible value of $\varepsilon_2(\omega)$ for energies lower than the bandgap (Figure 2h). Moreover, similarly to the case of SLR, thermal effects exhibit collective features, which ultimately leads to high and uniform temperatures in the limit of very large numbers of resonators (Figure 3f).[95,96] Photothermal effects can be engineered as useful sources of energy for applications, which indeed have given rise to the so-called field of thermoplasmonics,[97] for example, to increase the efficiency of solar-thermal processes (including solar steam generation) or the rate of thermally driven chemical reactions. Finally, the high Q-factor of the SLR may not be desired if the main target of the metasurface is efficient light harvesting across the entire solar spectrum. Therefore, metasurfaces exhibiting broadband optical absorption can be realized for instance by using metal/insulator/metal (MIM) structures.[15,98,99] This is further enhanced by employing a dissipative plasmonic material (high $\varepsilon_2(\omega)$) for the topmost layer, including TMNs (such as TiN) or other refractory metals (such as W, Ta, Mo), which also improves the performance under high temperature and harsh environmental conditions (Figure 3g) critical for solar-thermal applications such as TPVs.[100,101]

Dielectric metasurfaces are usually made of high refractive index semiconductors, such as Si, Ge, and TiO_2. They initially emerged as alternatives to plasmonic metasurfaces due to their reduced optical losses and higher Q-factors.[102] Similarly to plasmonic metasurfaces, SLRs in dielectric metasurfaces can be engineered by tuning the geometry of the metasurface (Figure 3h).[103] However, the constructive or destructive interferences of multipolar Mie resonances or of a single Mie resonance with another optical mode can lead to unusual effects in dielectric metasurfaces that are not observed in their plasmonic counterparts. For example, Fano resonances typically arise as interference between a discrete state and a continuum of states and appear as sharp and asymmetric peaks in transmission/reflection spectra.[104,105] Although Fano resonances can be also observed in plasmonic metasurfaces[106−108] and in a wide variety of systems,[109] they have been recently exploited in all-dielectric metasurfaces to achieve high Q factors. Fano resonances can be excited by breaking the symmetry of simple resonator geometries, as demonstrated with Ge cubes (Figure 3i), leading to Q factors as high as ∼1300 (numerically calculated, Figure 3j) or ∼600 (experimentally demonstrated with GaAs resonators).[110] A sort of special case of the Fano resonance is the classical analogue of electromagnetically induced transparency (EIT), which occurs when the frequencies of the two modes match and produces a sharp symmetric transmission peak in an otherwise opaque medium.[109,111] Further interesting effects are the so-called bound states in the continuum (BICs), which can be defined as theoretical states that lie in the continuum energy spectrum but remain localized in space and are associated with an infinite Q-factor.[112] Practical implementation of such a concept leads to the so-called quasi-BICs, which can be observed by engineering interference effects between different optical modes, similar to the case of Fano resonances.[113] For example, by tuning the aspect ratio of AlGaAs disk resonators in an all-dielectric metasurface (Figure 3k), the interference between Mie resonances and Fabry−Perot cavity modes was tuned achieving a quasi-BIC mode at ∼1570 nm with a Q-factor of ∼188 (Figure 3l). Even higher values ($Q\sim 5000$) have been recently achieved with asymmetric Si-based metasurfaces.[115] Such high Q-factors are especially interesting for optical sensing applications because they are associated with enhanced electric fields and narrow-band selectivity.[116] However, the so-obtained intense electric field may be exploited to increase the photogeneration rate in semiconductors for solar-energy conversion devices. Finally, a further example is the optical anapole,[117,118] which arises from the destructive interference between an electric dipole and a toroidal dipole and which could lead to high EM field enhancement in metasurfaces due to its nonradiating nature.

As an alternative to plasmonic and dielectric metasurfaces, hybrid plasmonic-dielectric metasurfaces can be realized[119] that synergistically exploit the strong light confinement and EM field enhancement of plasmon resonances and the low loss of Mie resonances.[120] Hybrid metasurfaces exhibit a high spectral tunability, which can be exploited to achieve broadband/perfect absorption or spectrally selective absorbers,[121] similar to MIM structures.[100] The tunability of the optical response of metasurfaces is indeed a very wide research field, which is described in details elsewhere (see refs 21, 31, 122, and 123 and references therein for a thorough treatment of such matter).

4. METHODS OF METASURFACE DESIGN

Designing metasurfaces for specific solar energy conversion applications involves the optimization of multiple structural and material parameters, including periodicity, geometry of the nanoresonators (orientation, size, and shape), and composition. In most cases, it is difficult to derive these parameters through analytical methods due to the complexity of the structure. Numerical simulations therefore play a crucial role in the design and optimization of metasurfaces by predicting the optical response and enabling the exploration of a wide range of parameters to identify optimal designs for specific applications. Since all the conventional numerical design methods begin with a predefined geometric structure to simulate its electromagnetic response, they are also categorized in the forward design approach.

With the advent of fast numerical methods for solving Maxwell's equations for complex environments, inverse design techniques have emerged as the next step in the evolution of EM design (see refs 40 and 126−131 for historical and comprehensive reviews and references therein). The inverse design procedure formulates the desired optical response as an objective function and uses optimization techniques, such as adjoint topology optimization, to find the optimal geometry and the dimensions of the metasurface.[132−140] This approach can handle complex functionalities and may not require prior knowledge of physical principles, making it a useful tool for gaining new insights.[141] The standard design process is typically executed through a combination of theoretical approaches, computational electromagnetic (CEM) simulations, or experimental methods (Figure 4a). However, with machine-learning methods, finding great traction in many branches of physics, specifically with deep-learning models (depicted as the blue box), we are now able to determine the EM response of a structure with orders of magnitude faster speed and high accuracy. Furthermore, deep-learning models are not limited to just forward problem solving. They also have the potential to

https://doi.org/10.1021/acsphotonics.3c01013
ACS Photonics XXXX, XXX, XXX−XXX

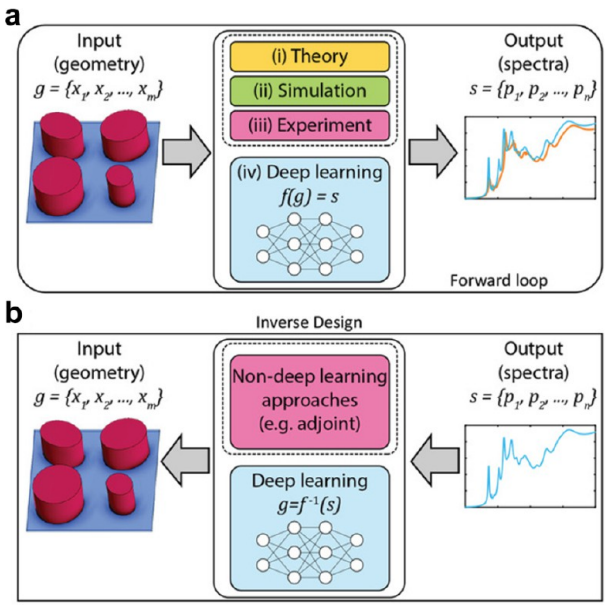

Figure 4. Schematic representation of (a) forward and (b) inverse electromagnetic design processes. The forward design approach begins with a predefined geometric structure, simulating its electromagnetic response. Conversely, the inverse design method starts with a desired electromagnetic response and then optimizes the structure to achieve the specified response. Adapted with permission from ref 141. Copyright 2021 Wiley-VCH.

tackle the "inverse problem". This involves training a model to predict the design that would result in a specific EM response as shown in Figure 4b. Despite the inherent difficulties of inverse modeling in comparison to forward modeling, its successful implementation could be a game-changer for material designers, offering them an innovative and powerful tool.

4.1. Conventional Design. Conventional numerical methods for solving Maxwell's equations, such as Finite-Difference Time-Domain (FDTD),[142] Finite-Difference Frequency-Domain (FDFD),[143] or Finite Element Method (FEM),[144] have been instrumental in simulating metasurfaces' optical responses.[145−147] The most commonly adopted metasurface design strategy involves generating a library of periodic meta-atoms with varying transmission amplitudes and phases by adjusting a few geometric parameters.[148−150] This is followed by generating an aperiodic metasurface by laying out the periodic meta-atoms according to the target, spatially varying the phase profile. However, this approach has two major limitations. First, the resulting metasurface should be almost periodic; thus, this strategy cannot be used to reliably design rapidly varying phase profiles. Second, generating the metasurface library becomes increasingly difficult for multifunctional design problems.[149,151] Consequently, the conventional forward design strategy based on phase matching may not be useful or even applicable in many cases, such as when targeting phase profiles cannot be analytically retrieved or is a multiwavelength/function operation.[8] As the device functionality, design constraints, and degrees of freedom scale up, the success of metasurfaces demands the development of inverse design methods.

4.2. Topology Optimization. Inverse design methods of metasurfaces largely employ both gradient-free and gradient-

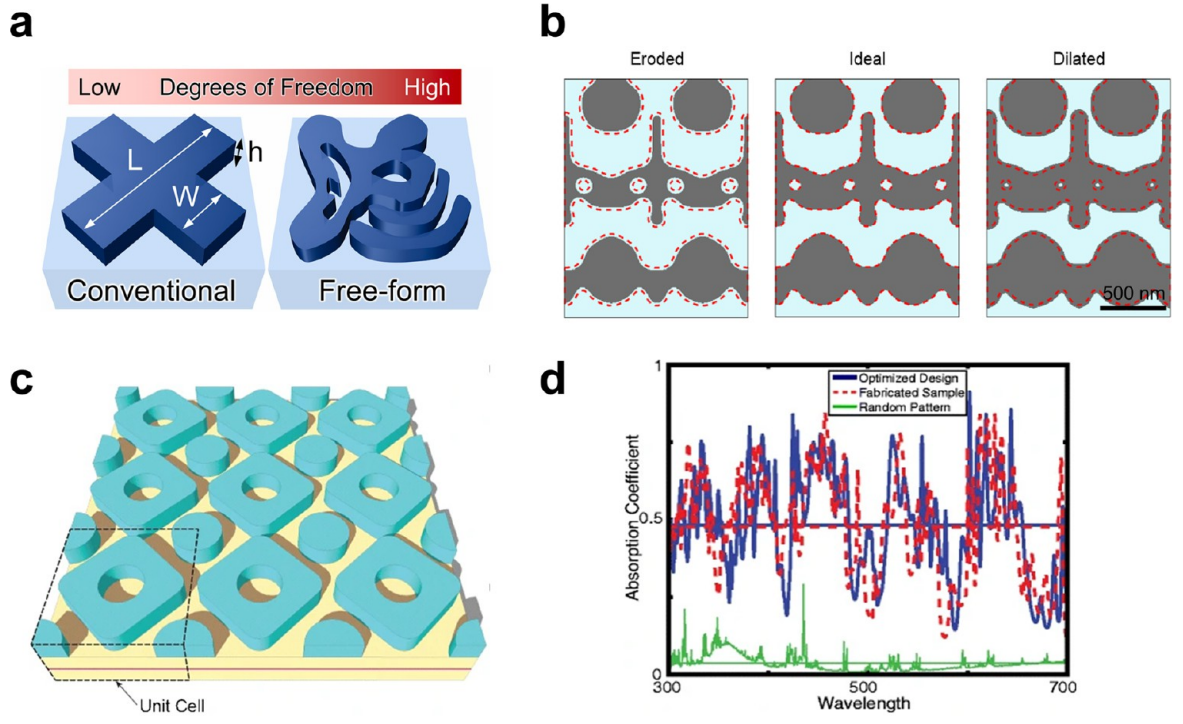

Figure 5. Topology optimization methods for metasurfaces. (a) Degrees of freedom comparison between conventional (left) and free-form (right) design (topology optimization) schemes. Reproduced from ref 157. Copyright 2022 author(s), licensed under a CC-BY Creative Commons Attribution 4.0 License. (b) Schematic of the representative topology-optimized metasurface, in which the ideal pattern is eroded and dilated with edge deviations of -10 and +10 nm, respectively. Adapted with permission from ref 136. Copyright 2019 Optical Society of America. (c) Nanophotonic light-trapping structure illustration and (d) its broadband optimization results using genetic algorithm (GA) based nongradient topology optimization (NGTO) for the high-permittivity scattering material case. (c, d) Reproduced with permission from ref 156. Copyright 2014 Springer-Nature.

https://doi.org/10.1021/acsphotonics.3c01013
ACS Photonics XXXX, XXX, XXX−XXX

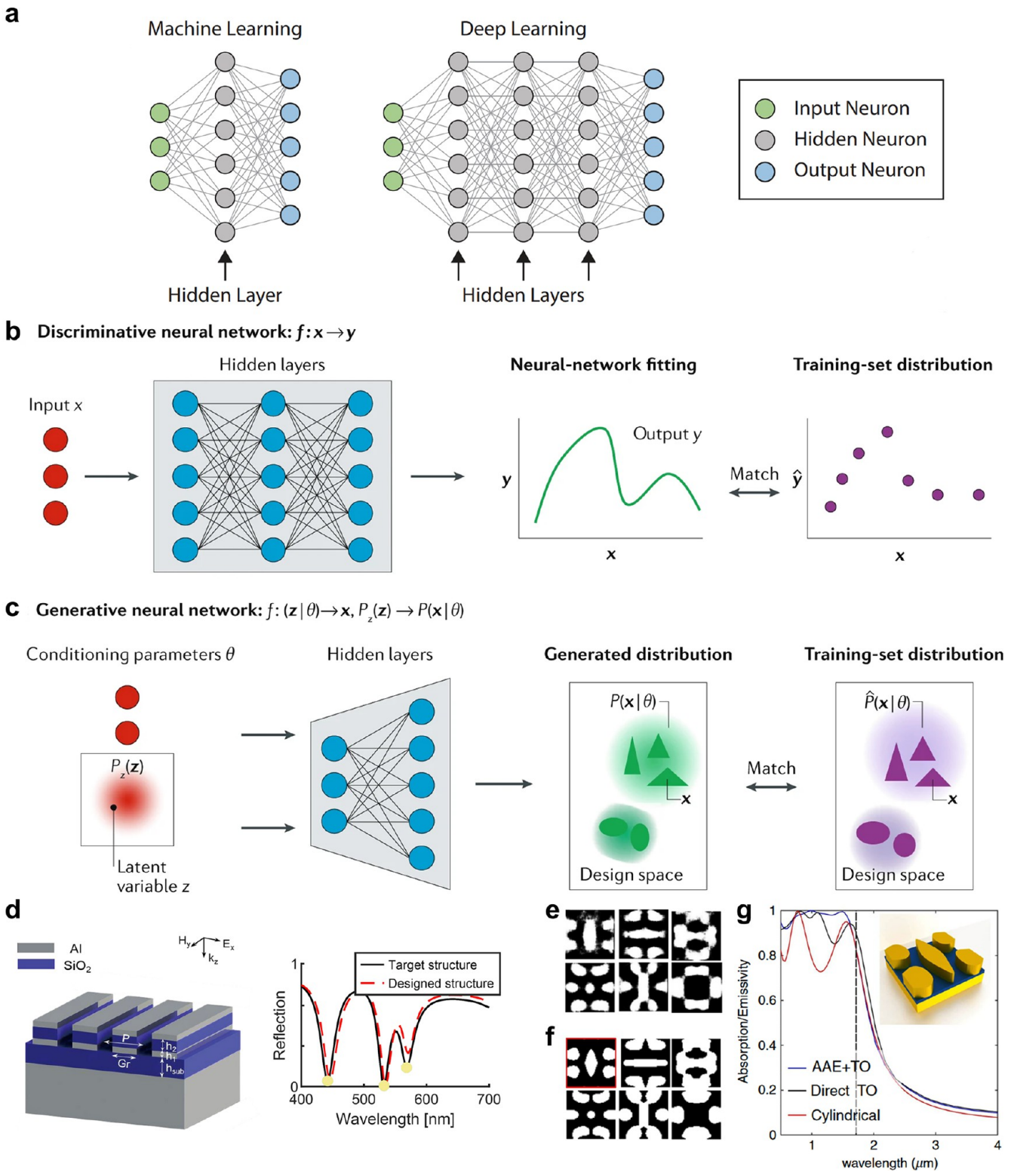

Figure 6. Deep-learning assisted design methods for metasurfaces. (a) Schematic illustration of machine learning and deep learning. Adapted with permission from ref 182. Copyright 2022 Elsevier. (b) Schematic illustration of discriminative neural networks and (c) generative neural networks. (b, c) Reproduced with permission from ref 132. Copyright 2021 Springer-Nature. (d) Schematic and optical reflectance of a perfect multiband absorber designed by an artificial neural network. Reproduced from ref 180. Copyright 2021 Chinese Laser Press. (e) Examples of designs generated by trained adversarial autoencoders (AAEs) and (f) the same after the structure refinement process by topology optimization (TO). (g) Absorption/emissivity spectra of the best AAE + TO design in the set, the best direct TO design, and an optimized cylindrical emitter. The inset shows the unit cell configuration of the best design in the set. (e–g) Adapted with permission from ref 172. Copyright 2020 AIP Publishing.

based optimization techniques. Gradient-free methods, although slower, can find global optima, handle discrete parameters and nondifferentiable objectives, and evade the local minimum trapping often encountered in gradient-based

https://doi.org/10.1021/acsphotonics.3c01013
ACS Photonics XXXX, XXX, XXX−XXX

methods. Conversely, gradient-based methods, with their rich local gradient information, converge much faster, but they require knowledge of cost function derivatives with respect to design parameter.[152] As a gradient-based optimization technique, topology optimization is used to determine the optimal layout of a two- or three-dimensional system, such as material density distribution inside a nanophotonic device.[134,153] It works by defining the design using a pixel representation, with each pixel containing a discrete or continuous parameter that needs adjustment, aiming to maximize a target merit function using gradient descent.[154] At each iteration, the required modification for every pixel's material is calculated by comparing the present condition of the device with a desired outcome. This can be achieved using either an analytical approach or adjoint analysis.[155] Methods such as adjoint analysis enable the number of simulations required for topology optimization to stay fixed as the number of elements in the system grows, allowing for high-resolution, curvilinear structures containing thousands to millions of elements.[126] Thus, it provides a large degree of design freedom, which can lead to nearly arbitrary shapes[135] (Figure 5a). One of the key advantages of topology optimization for photonic inverse designs is the ability to discover nonintuitive device layouts that traditional methods cannot access.[8] Moreover, topology optimization improves the metasurface performance by expanding the design domain. Another advantage of topology optimization is that it can predict errors or inevitable inaccuracies in the fabrication process of real devices, therefore enhancing the robustness of the simulated design. For example, Wang et al. addressed the robustness issue in a topology-optimized metasurface design to overcome the sensitivity of the optimal geometry to fabrication errors and deviations from the design parameters (Figure 5b).[136] Topology optimization could also address solar energy conversion problems that are of interest to this review. Yu et al. applied a genetic algorithm (GA) based nongradient topology optimization (NGTO) for designing highly efficient nanophotonic light-trapping structures in solar cells beyond the reach of conventional intuitive designs (Figure 5c).[156] The proposed approach demonstrated robustness in achieving highly efficient designs using scattering materials of both low and high permittivity, either for a specific wavelength or across a wide range of wavelengths (Figure 5d).

One limitation of topology optimization is that it is fundamentally a local optimization process. Thus, for problems where the design space is barely large enough for the desired functionality, sophisticated search strategies may be required, such as multistart algorithms[158] or deterministic global optimization methods.[159] Another challenge is the high computational costs stemming from the repetitive use of full-wave solvers. Thus, global optimizers coupled with novel EM solvers with substantially less computational cost are needed to take the next step in photonic inverse design.

4.3. Deep-Learning Assisted Design. Machine learning has emerged as a powerful method for computer vision,[160] speech recognition,[161] natural language processing,[162] robot control,[163] and more. Deep learning based on multilayer artificial neural networks (Figure 6a)[164] has recently attracted significant attention from the photonics' community.[165] Deep learning that brings substantial acceleration capability and forth a feasible avenue for global optimization, has been introduced in metasurface design problems, including multilayer perceptrons,[166,167] convolutional neural networks,[168] generative adversarial networks,[169] and variational autoencoders.[170−172] The method allows combination with other optimization techniques such as genetic algorithms,[173,174] topology optimization,[171,172] or adjoint optimization[172,175] to enable high-performance, large-scale metasurface designs.

Presently, two types of deep learning have been used in metasurface design: discriminative networks and generative networks. Discriminative networks (Figure 6b) are supervised learning algorithms that accurately map the explicit relationship between metasurface geometry and its electromagnetic response.[128] Discriminative networks used as high-speed EM solvers can calculate the electromagnetic response of system orders of magnitude faster than classical numerical methods.[176] Generative networks (Figure 6c), on the other hand, are unsupervised learning algorithms to generate new metasurface structures with desired electromagnetic properties.[39,169,177] By mapping a standard probability distribution to multiple potential designs, generative networks enable better optimization by more extensive design space exploration.

To substitute the classical EM solver with efficient discriminative networks, Sullivan et al. developed a deep neural network to emulate the outputs of FDTD simulations, which is the foundation of rapid microstructure design optimization for thermal radiation control.[178] Trained discriminative networks have also been shown to optimize nanophotonic devices,[8] also for applications in the energy conversion field. The model from Du et al. assisted in discovering nonintuitive relationship between the moth-eye metasurface and optical responses, and then efficiently designed a metasurface with ultrabroadband antireflection and nonlinear function of reflectivity.[179] So et al. also reported a deep learning method, which facilitates highly robust spectrally sensitive multiband absorbers that has a low average mean squared error (MSE, Figure 6d).[180]

When it comes to the generative networks application in desired metasurface designs, Ding et al. established a model by the combination of convolutional variational autoencoder and deep neural network[181] to realize ultrabroadband, low-profile absorbers design.[181] In addition, generative networks have been combined with topology-optimized designs for the rapid generation of highly efficient metasurface designs. Kudyshev et al. introduced several methods that combine topology optimization with deep learning approaches for the inverse design of metasurface thermal emitter for TPV applications (Figure 6e−g).[172]

5. APPLICATIONS OF METASURFACES IN SOLAR ENERGY CONVERSION PROCESSES

Devices enabling the use of the full solar spectrum and mitigating the intermittent characteristic of sun light availability are key to attaining a reliable and renewable cycle based on solar energy. On one hand, PV cells enable direct input of electricity, while photocatalytic processes allow the conversion from solar energy to fuels or chemicals unlocking the transport, storage, and delayed consumption of energy. On another hand, photothermal processes transform solar energy to thermal energy facilitating direct (i.e., steam engine) and indirect (i.e., enhancement rate for chemical reactions) pathways for energy transduction. This section focuses on the existing applications of metasurfaces for solar energy conversion divided into four categories: photovoltaics, solar-to-thermal processes, catalytic processes, and radiative cooling.

5.1. Metasurfaces for Photovoltaics. Over the past decades, extensive research focused on the development of (ultra)thin film PV cells to improve scalability and cost

https://doi.org/10.1021/acsphotonics.3c01013
ACS Photonics XXXX, XXX, XXX−XXX

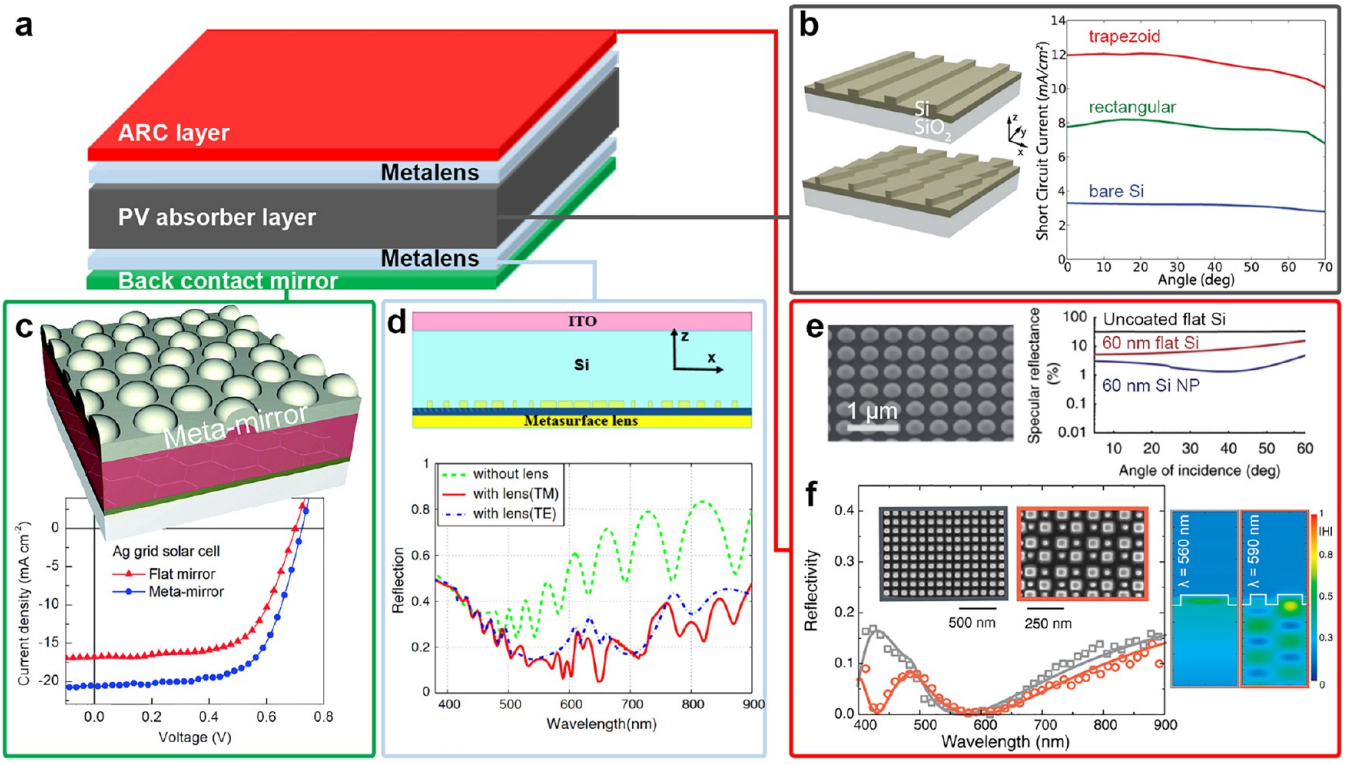

Figure 7. Metasurfaces' applications in photovoltaic cells. (a) The different parts of the PV cell where metasurfaces can impact the photovoltaic properties. (b) Impact of the shape of the Si Mie resonator metasurfaces on the short circuit current. Adapted from ref 187. Copyright 2016 Author(s), licensed under a CC-BY Creative Commons Attribution 4.0 License. (c) Back reflector of Al meta-mirror on an organic PV device with Ag microwire grid. Adapted with permission from ref 190. Copyright 2016 The Royal Society of Chemistry. (d) Silicon nitride/aluminum metalenses enhance the PV device's broadband light absorption. Reproduced with permission from ref 191. Copyright 2018 The Optical Society. (e, f) Antireflective coatings based on Si Mie resonators with (e) different thicknesses and (f) different geometries inside the metasurface arrays. (e) Adapted with permission from ref 193. Copyright 2012 Author(s), licensed under a CC-BY-NC-ND Creative Commons Attribution 3.0 License. (f) Adapted with permission from ref 194. Copyright 2018 American Chemical Society.

effectiveness (e.g., organic polymers, perovskites, semiconductors, transition metal dichalcogenides, plasmonic metals, etc.).[183−185] However, thin PV devices exhibit a lower power conversion efficiency in comparison with standard *c*-Si PV cells; thus, several strategies were developed to enhance light absorption within the thin PV layer. One promising approach is to use metasurfaces to enable enhancement on different parts of a PV cell (Figure 7a; see Table S1 for additional details).

The adoption of dielectric Mie resonators, notably Si-based ones, enabled impressive enhancement in broadband absorption while keeping nanometric thicknesses. Tailoring nanoresonators' size and shape (e.g., nanodimers, nanopillars, rectangular, and trapezoidal metasurfaces)[186−188] effectively controls the absorption properties. For example, a silicon-on-insulator Schottky barrier photodetector was fabricated as a prototype thin film solar cell and modified with arrays of Si nanoresonators with rectangular and trapezoidal shapes (Figure 7b).[187] While the metasurface design based on rectangular pattern already led to a significant enhancement of the short circuit current density compared to the flat structure (i.e., 7.8 vs 3.2 mA cm^{-2}), the best performance was achieved with trapezoidal nanoresonators (i.e., 12.0 mA cm^{-2}, Figure 7b). Such a result was attributed to the presence of several coupled resonances producing broadband optical absorption and enhancing the photocurrent, such as localized Mie modes at shorter wavelengths (λ < 500 nm) and waveguide modes at longer wavelengths (λ > 600 nm).

Metasurfaces can also be adopted in the additional layers to improve the overall performances of the cells, e.g., back reflecting meta-mirrors (BRMs), metalenses, or antireflective coatings (ARCs). In BRMs, the electric field is weakened at the near-surface region corresponding to a quarter of the incident wavelength, which becomes considerable for thin films.[189] Metasurfaces (i.e., meta-mirrors) solve this problem by enhancing the electric field in this near-surface region. For example, Ou et al. integrated Al meta-mirrors on the photoactive layer observing an increase in light harvesting in the near-UV to near-IR (26.2%) with 9.5% enhancement in power conversion efficiency in comparison with flat Al mirrors (Figure 7c).[190] Using a different approach, metasurfaces acting as metalenses can be used to modify the wavefronts of the incident light driving the field enhancement in the active layer of the PV cell. Thus, metalenses were demonstrated as an interesting strategy to boost the light absorption and the short circuit current of the PV cell. A reflective metalens (Si_3N_4/Al) integrated at the bottom of a Si thin film cell enabled to focus/trap the light inside the PV absorber layer enhancing the short circuit current ∼1.4 times (Figure 7d).[191] Metamaterials can also solve the light loss due to reflection thanks to metasurface ARCs placed at the top of the cell, which trap the light back inside the PV absorber layer.[192] Recent studies have shown the possibility of employing dielectric metasurfaces as ARCs. Notably, Spinelli et al. demonstrated, through Si nanodisk metasurface, the possibility to reach almost zero total reflectance in a broad spectral range with incident angle up to 60° (Figure 7e).[193] Furthermore, Mie nanoresonators used in sufficiently low densities improved the antireflection properties due to destructive interferences.[194]

https://doi.org/10.1021/acsphotonics.3c01013
ACS Photonics XXXX, XXX, XXX−XXX

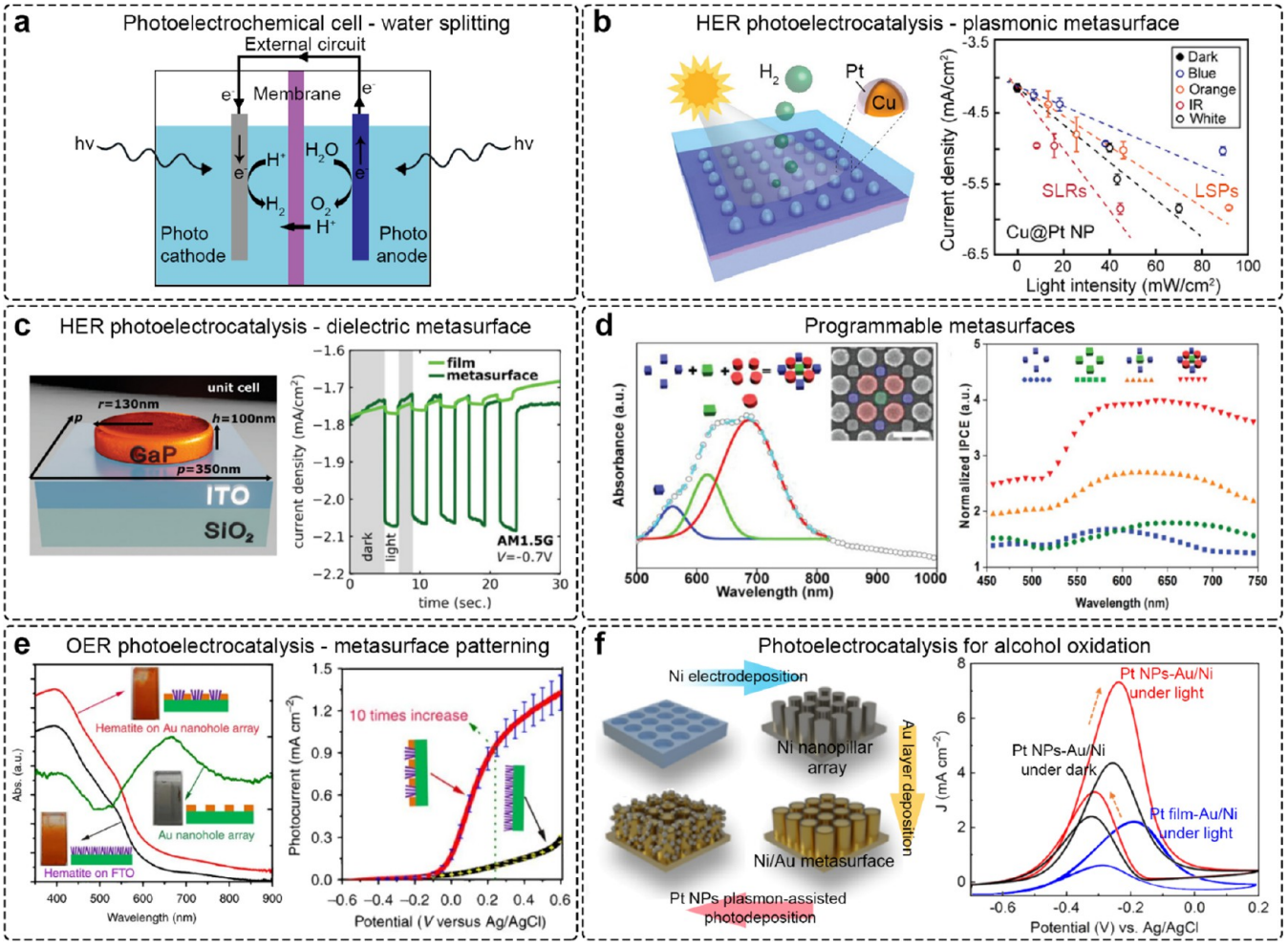

Figure 8. Metasurfaces' applications in photoelectrocatalysis. (a) Scheme of a typical PEC cell. (b) Impact from individual LSPRs and collective SLR modes on HER production from core−shell Cu/Pt lattices. Reproduced with permission from ref 205. Copyright 2021 American Chemical Society. (c) Enhancement of HER production from dielectric metasurface compared to thin films. Reproduced with permission from ref 35. Copyright 2021 Author(s), licensed under a CC-BY Creative Commons Attribution 4.0 License. (d) Impact of multisubset programmable Au NP superlattices on the light absorption. Reproduced with permission from ref 206. Copyright 2020 author(s), licensed under a CC-BY Creative Commons Attribution 4.0 License. (e) Enhancement of the OER photocatalysis from Au nanohole arrays with Fe_2O_3 nanowires grown inside the nanoholes. Reproduced with permission from ref 207. Copyright 2013 Springer Nature. (f) Plasmonic Ni/Au−Pt metasurfaces for methanol oxidation applied in direct alcohol fuel cell. Adapted with permission from ref 208. Copyright 2022 Wiley-VCH GmbH.

Pecora et al. have shown that such effect can exceed the geometrical size of the nanoresonators implying the possibility to integrate different units inside the ARC metasurface to manage the antireflection of broader spectral range (Figure 7f).[194] Another potential advantage of ARC metasurfaces lies in the possibility of applying them to standard solar cells as an alternative to pyramidal textures, which are commonly used in Si solar cells but are not compatible with thin and flexible absorbers. For instance, Piechulla et al. fabricated a disordered metasurface made of TiO_2 disks (370 nm in diameter) by a scalable colloidal method on top of a standard heterojunction Si solar cell.[195] Such a structure showed a significant reflection suppression and could also be applied to other cell architectures and materials. In addition, such ARCs also enable color customization of the solar panel thanks to the high control over the reflected light, which answers to industrial needs to reach consumer aesthetic requirements.[196] Alternatively to ARCs, metasurfaces can induce light-trapping effects in the photoactive layer of thin-film or organic solar cells,[197,198] which typically suffer from high transmission losses. In this regard, plasmonic metasurfaces may be employed rather than dielectric ones. For example, Voroshilov et al. integrated a plasmonic metasurface made of Ag nanoantennas embedded in the PV layer (bulk-heterojunction based on phthalocyanine as a donor and fullerene as an acceptor). Despite introducing several side effects (such as shading of photoactive area and recombination of charge carriers), the Ag nanoantennas induced an electric field enhancement that increased the optical absorption and, as a result, the power conversion efficiency of the device by a remarkable 18%.[199]

5.2. Metasurfaces for Catalytic Processes. Solar energy can be converted to chemical energy through photocatalysis, which allows to stock and transport energy. On one hand, extensive efforts focused on essential molecules for environment and energy areas (i.e., H_2 production, CO_2 reduction, ammonia production, etc.) showed promising advances.[200,201] On the other hand, research on photoreforming from biomass waste is exponentially growing to provide a renewable and clean source for energy and chemical production.[202,203] The most mature and popular photocatalytic process is the water splitting process,

https://doi.org/10.1021/acsphotonics.3c01013
ACS Photonics XXXX, XXX, XXX−XXX

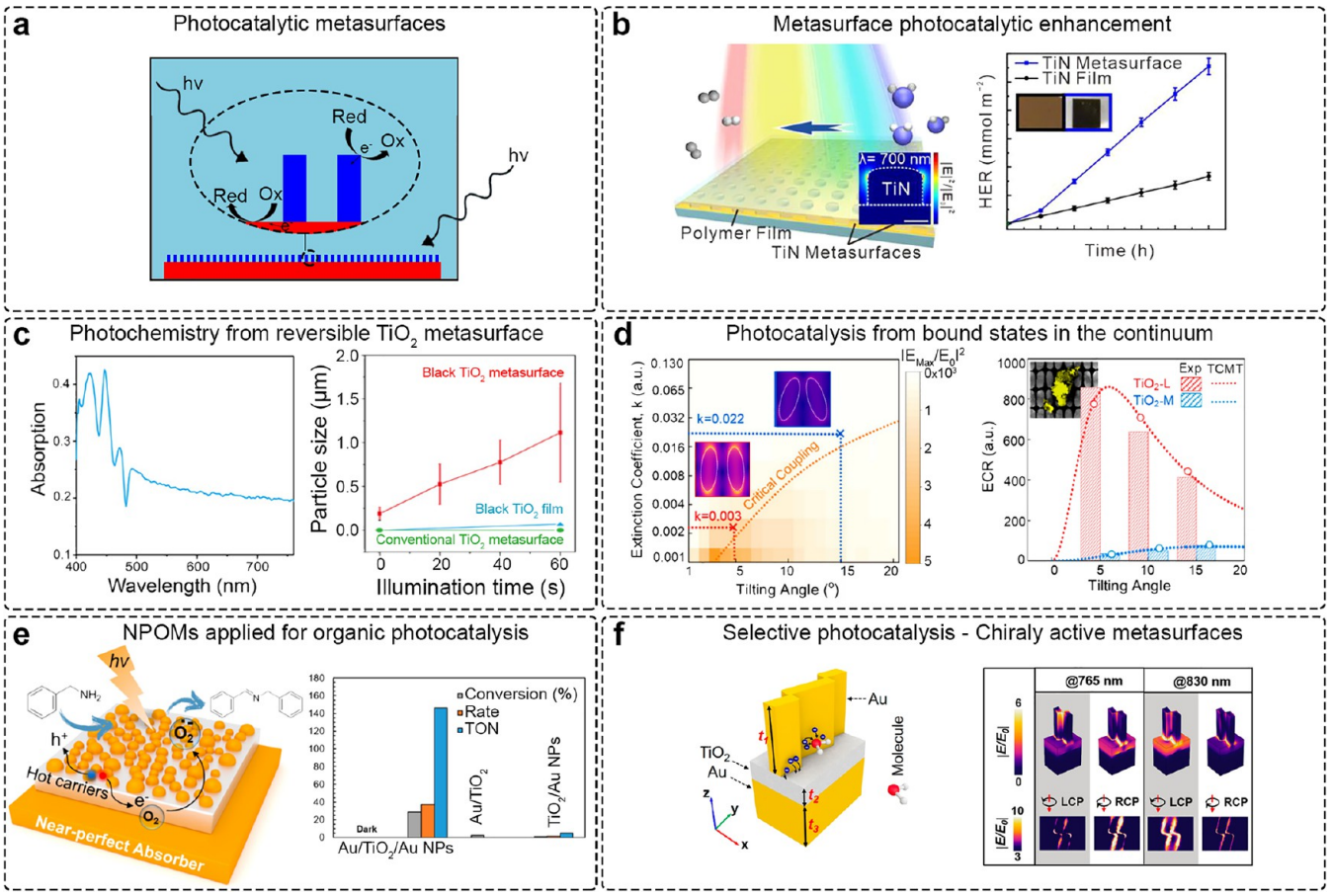

Figure 9. Metasurfaces' applications in photocatalysis. (a) Scheme of the photocatalytic metasurface principle. (b) TiN metasurfaces versus TiN film effect on the photocatalytic efficiency enhancement. Reproduced with permission from ref 34. Copyright 2021 American Chemical Society. (c) Reversible TiO_2 metasurface, from conventional to black TiO_2 and backward, applied to photochemistry. Adapted with permission from ref 210. Copyright 2019 Author(s), licensed under a CC-BY Creative Commons Attribution 4.0 License. (d) Photocatalysis for the formation of silver NPs from TiO_{2-x} BIC metasurfaces. Adapted with permission from ref 211. Copyright 2022 Author(s), licensed under a CC-BY-NC-ND Creative Commons Attribution 4.0 License. (e) NPOMs Au metasurface on a TiO_2/Au mirror for organic photocatalysis through hot-carrier generation. Reproduced with permission from ref 212. Copyright 2018 American Chemical Society. (f) Chiral metasurfaces were applied to tune the photocatalysis selectivity and hot-spots position. Adapted with permission from ref 213. Copyright 2019 American Chemical Society.

consisting of breaking water molecules into hydrogen (H_2) and oxygen (O_2), where the former can serve as a renewable and clean fuel source. Generally, PEC cells are used as half reaction cells with the water oxidation and water reduction separated at the photoanode and photocathode (Figure 8a and Table S2 for additional details).

Metasurfaces improve the light absorption and charge carrier generation in the semiconductor material by means of intense electromagnetic fields excited by collective effects, e.g., SLRs (Figure 3).[204] For instance, a metasurface based on bimetallic nanounits, i.e., Cu particles coated with Pt as the HER catalyst, demonstrated SLRs arising at ~865 nm. The collective modes combined with the plasmonic properties of Cu particles (LSPR at ~675 nm) enabled broad solar absorption up to the NIR (Figure 8b).[205] Interestingly, SLRs showed a 2-fold activity enhancement over the LSPRs, highlighting the strength of SLRs both on the solar absorption and the enhanced near-field intensities. Similarly, Hüttenhofer et al. featured amorphous GaP nanoantenna metasurfaces, which presented individual anapole and collective SLR modes (Figure 8c).[35] They compared the HER activity of the metasurface and the reference thin film following a 1.5 nm Pt layer deposition (Figure 8c). The metasurface demonstrated a 5.7 enhancement factor in comparison with the flat film, which identified as a combination of the anapole and SLR modes.[35] Interestingly, Xu et al. built nanoparticle superlattices with different geometrical subsets of Au NPs to simultaneously exploit the different resonances associated with each subset configuration (Figure 8d).[206] Such a so-called programmable metasurface demonstrated that a photoanode based on multiple subsets of CdS particles improved the PEC performance (i.e., IPCE) accordingly with the increase in optical absorption. Therefore, these results illustrate the impressive degree of control on the photoelectrode performance by means of metasurface engineering and their correlated SLR modes. Likewise, the use of an Au nanohole metasurface (with ~350 nm diameter and ~490 nm periodicity) produced an increase of optical absorption and a 10-fold enhancement in the photocurrent produced by a hematite (α-Fe_2O_3) photoanode compared to the same without the Au metasurface (Figure 8e).[207] These observations were ascribed to the excitation of surface plasmon polariton modes at 350−550 nm and the consequent excitation of waveguided modes in the hematite nanorods (acting as waveguides) by interband transitions. Overall, these works highlighted the interesting prospects of metasurfaces for improving PEC performances through collective modes. Apart from water splitting, other

https://doi.org/10.1021/acsphotonics.3c01013
ACS Photonics XXXX, XXX, XXX−XXX

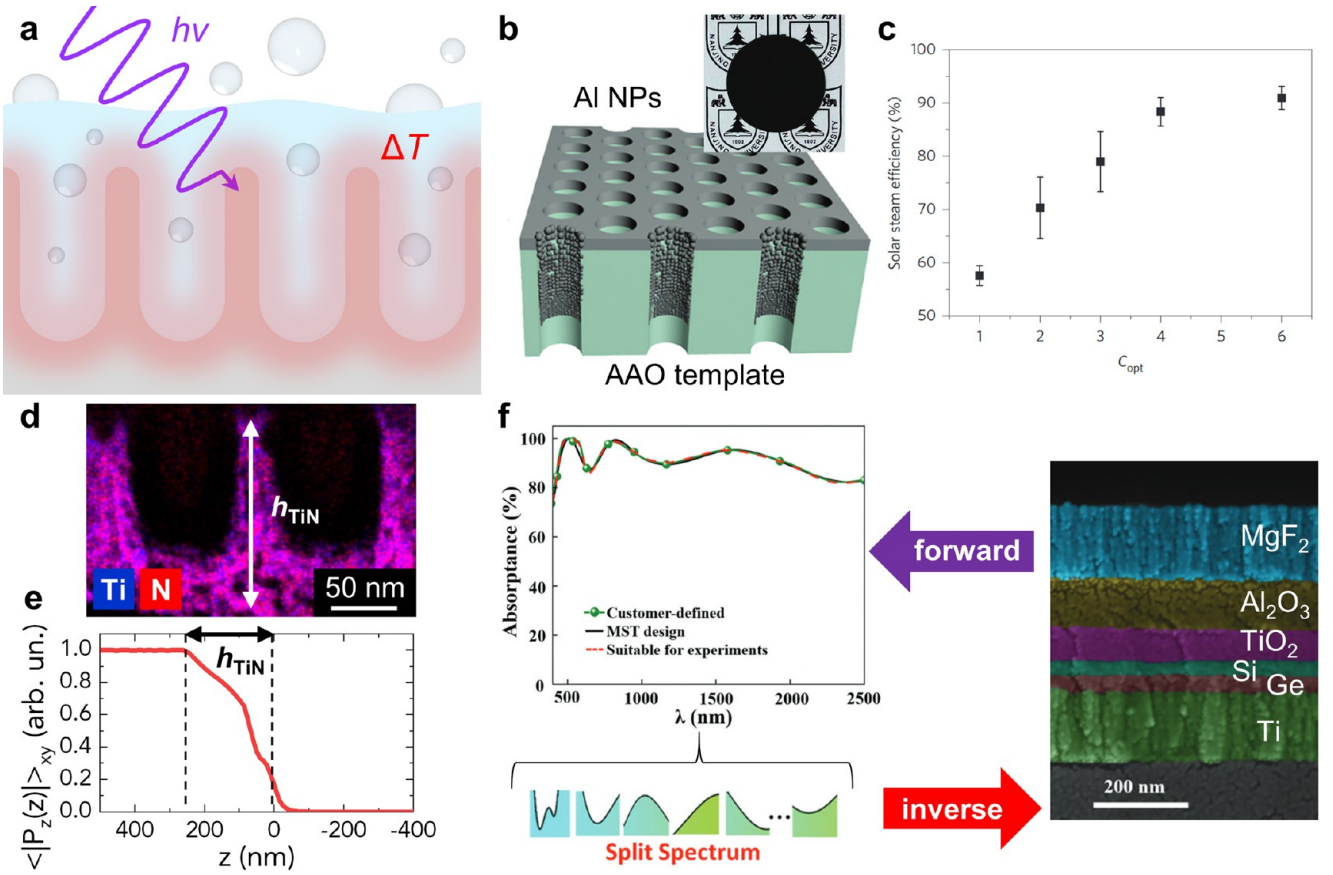

Figure 10. Metasurfaces for low-temperature solar-thermal conversion. (a) Schematic of solar steam generation driven by a metasurface. (b) Schematic of an anodic aluminum oxide (AAO) template coated by Al nanoparticles (inset: optical photograph of the same) and (c) solar steam generation efficiency of the same under concentrated solar light (1−6 Suns). Reproduced with permission from ref 223. Copyright 2016 Springer Nature. (d) High-resolution TEM-EDS mapping and (e) optical power absorption (vertical component of the Poynting vector averaged over horizontal planes) of TiN nanocavities. Reproduced with permission from ref 227. Copyright 2021 Elsevier. (f) Schematic of model employing forward and inverse design to engineer a multilayer metamaterial absorber (right: cross-sectional SEM image). Adapted with permission from ref 228. Copyright 2023 Author(s), licensed under a CC-BY Creative Commons Attribution 4.0 License.

processes can benefit greatly from the photonic designs brought by metasurfaces. For example, plasmonic metasurfaces consisting of Au/Ni nanopillars were used to grow Pt NPs as catalytic material on the electromagnetic hot spots (Figure 8f).[208] The so-obtained Pt−Au/Ni metasurfaces were used for methanol oxidation in direct alcohol fuel cells, revealing a significant enhancement in electrocatalytic activity under light irradiation compared with a continuous Pt film deposited on the Au/Ni metasurfaces (Figure 8f).[208] Follow-up studies evidenced that catalytic Pd particles grown at the EM hot spots led to a higher catalytic activity and stability compared to the same photoanode where the NPs were grown in a homogeneous way on the whole surface area of the structure.[209]

Metasurfaces have also been employed in photocatalytic arrangement, where no bias is applied, and the oxidation and reduction half-reactions occur at the solid−liquid interface of the same illuminated material in contact with the electrolyte (Figure 9a and Table S3 for additional details). In this regard, plasmonic and dielectric metasurfaces can lead to different effects to enhance the performance of the device, which is usually evaluated in terms of the H_2 production rate. On the one hand, plasmonic metasurfaces can enhance the photocatalytic activity of an adjacent photocatalyst (semiconductor) material. On the other hand, metasurfaces based on metal oxides can exhibit an intrinsic photocatalytic activity, which can be enhanced by higher absorption or by specific resonance modes produced by the metasurface morphology. As an example of the first category, Yu et al. engineered a TiN metasurface exhibiting broadband optical absorption in the visible range (i.e., ∼92% in the 400−750 nm range) and coated it with a polymeric photocatalyst to perform H_2 production experiments under visible-light irradiation (Figure 9b).[34] The observed performance was 3-fold higher compared with a TiN flat film and was attributed to a combination of hot carrier transfer and thermal effects induced by the plasmonic metasurface. As an example of the second category, a TiO_2 metasurface could be reversibly switched from oxidized state to reduced state (i.e., black TiO_2 or TiO_{2-x}) to increase the absorption spectrum by ion implantation.[210] The black TiO_2 metasurface exhibited substantially higher photocatalytic activity compared to a flat black TiO_2 film as well as a white TiO_2 metasurface, as monitored by the photoreduction of Ag NPs from $AgNO_3$ solution (Figure 9c). In a follow-up study, the extinction coefficient and the geometry of ellipsoidal nanoresonators of TiO_2 metasurfaces were engineered to excite *quasi*-BICs (see also section 3.2).[211] Contrary to the previous example, TiO_2 metasurfaces with the lowest defect concentration exhibited the highest photocatalytic activity (also in this case measured by the photodeposition of Ag NPs) thanks to the electric field

https://doi.org/10.1021/acsphotonics.3c01013
ACS Photonics XXXX, XXX, XXX−XXX

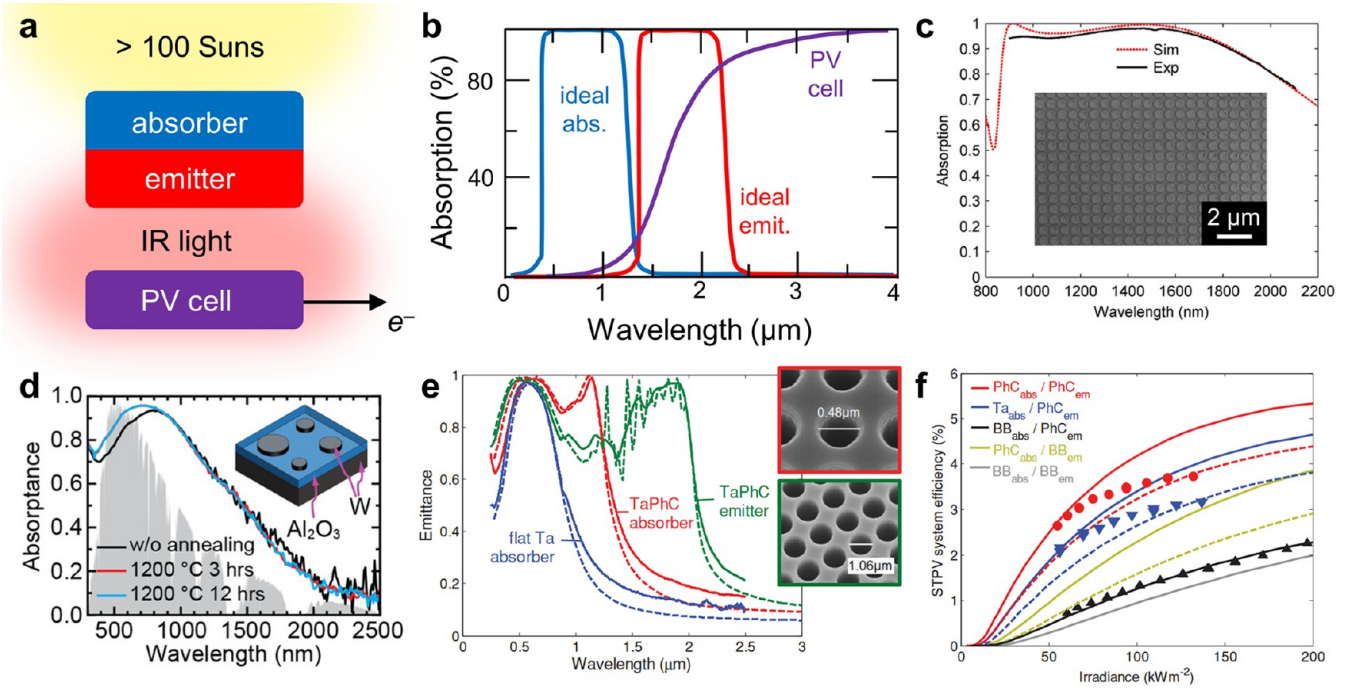

Figure 11. Metasurfaces with high spectral selectivity are used for TPV applications. (a) Schematic of a TPV system and (b) optical spectra of an ideal absorber, ideal emitter (operating at 1500−2000 K) and PV cell underneath. (c) Broadband absorption in a Ti disk array/SiO_2/Au metasurface. Adapted with permission from ref 101 Copyright 2016 Author(s), licensed under a CC-BY Creative Commons Attribution 4.0 License. (d) Thermal stability of a W-based metasurface absorber. Reproduced with permission from ref 229. Copyright 2018 American Chemical Society. (e) Normal emittance spectra (experimental data retrieved by reflectance measurements, solid lines; numerical data, dashed lines) and SEM images of Ta-based photonic crystal (PhC) absorber (red) and emitter (green) compared to flat Ta absorber (blue), all coated with HfO_2. (f) Measured (symbols) and simulated (lines) TPV efficiency for different absorber/emitter pairs (PhC: photonic crystal; Ta: flat Ta; BB: blackbody). (e, f) Adapted with permission from ref 230. Copyright 2014 Wiley-VCH.

enhancement produced by *quasi*-BICs, leading to resonant absorption (Figure 9d).

It should be noted that a wide variety of photocatalytic reactions can benefit from optical enhancement phenomena arising in metasurfaces. For example, the photocatalytic oxidation of benzylamine into the corresponding imines was performed on nanoparticle-on-mirrors (NPoMs, Au NPs/TiO_2/Au mirror) with near-perfect absorption (94%) showing up to 29-fold enhancement in the reaction rate compared to control samples (Figure 9e).[212] We expect such research applied to organic chemistry to soar in the next decades, as the need for a clean source of chemical production is a necessity. Another important aspect enabled by photonic engineering concerns the product selectivity in photocatalytic reactions. For example, plasmonic metasurfaces based on chiral nanoresonators enabled concentrating electromagnetic hot-spots on different areas of the nanostructure depending on the polarization of the incident light (Figure 9f).[213] The use of chiral nanostructures can enable, for instance, enantioselective photoprocesses and enhanced product selectivity bringing valuable perspectives to the chemical industry.[214]

Ultimately, material and geometry optimization of a metasurface design plays a critical role to improve the library of photocatalysts components.[34,64,205,210,215−217] In this regard, machine-learning and inverse-design methods emerged as innovative tools to tackle this challenge of exponential possibilities.[172,218,219]

5.3. Metasurfaces for Solar-Thermal Processes. The energy of the incident light is eventually dissipated to the environment either nonradiatively, via heat conduction, or radiatively, via thermal radiation. The first scenario gives rise to photothermal effects, which are particularly relevant in plasmonic metasurfaces due to their high optical absorption mediated by free carriers (Section 3.2). Such a mechanism can be exploited for various solar-thermal applications. As a widely investigated solar-thermal process at a low temperature regime, solar steam generation[220−222] makes use of a broadband solar absorber to promote water evaporation under solar irradiation (Figure 10a and Table S4 for additional details). This technology requires the use of simple and scalable photothermal materials to ensure its application in decentralized scenarios. Inexpensive material structures that resemble plasmonic metasurfaces can be realized by coating self-assembled anodic aluminum oxide (AAO) templates with Al, Au, or TiN.[223−225] For example, the wide pores of a 3D AAO template (~300 nm diameter) allowed deposition of Al by evaporation, forming close-packed NPs on the inner walls of the pores and a thin compact layer on the top, leading to nearly unitary absorptance in the 300−1500 nm range (Figure 10b).[223] The porous nature of such material allowed paths for efficient water supply and steam flow while floating. As a result, over 90% solar-to-vapor efficiency under moderate light concentrations (i.e., 6 Suns) was achieved (Figure 10c). Similar results were obtained by investigating AAO templates with different pore sizes (50−400 nm) coated with TiN by sputtering (80 nm nominal thickness).[225] Alternatively, AAO templates can be coated with reduced metal oxides instead of metals as photothermal materials, such as an ultrathin (2−10 nm range) amorphous TiO_x layer achieved by atomic layer deposition (ALD) leading to ~95% optical absorption in the 300−1600 nm range.[226] With

https://doi.org/10.1021/acsphotonics.3c01013
ACS Photonics XXXX, XXX, XXX−XXX

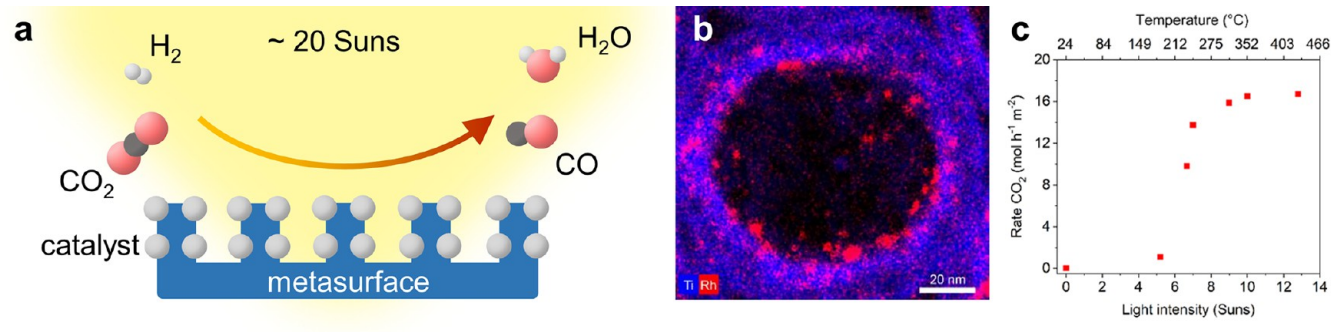

Figure 12. Metasurfaces for photothermal catalysis. (a) Schematic illustration of photothermal catalysis (reverse water gas shift reaction, RWGS) driven by plasmonic metasurfaces. (b) High-resolution TEM-EDS mapping of TiN nanocavities decorated with Rh nanoparticles and (c) application of the same in the CO_2 oxidation reaction. (b, c) Reproduced with permission from ref 235. Copyright 2020 American Chemical Society.

the idea of further concentrating the optical power in a plasmonic metasurface layer, a recent work introduced self-assembled nanotube arrays obtained by anodization of a Ti foil and further nitridation in NH_3 atmosphere, leading to long-range ordered nanotubes featuring TiN stoichiometry (Figure 10d).[227] Electromagnetic simulations by FEM demonstrated a confinement of light power absorption within the height of the nanotubes (~250 nm, Figure 10e), which was ascribed to collective photothermal effects produced by plasmonic and cavity modes in the ordered TiN nanotubes. The proposed material exhibited promising water evaporation performance (maximum ~76% solar-to-vapor efficiency at 15 Suns) and great potential for broader applications requiring fast heat transfer dynamics. In contrast with most of experimentally focused studies, a recent work presented an original method taking advantage of both the forward and inverse design approaches to design a multilayer metamaterial absorber (Figure 10f).[228] A customer-defined absorption spectrum was used as a target and "split" into different wavelength sections. The inverse design was used to predict the thicknesses of the layers constituting the metamaterial, which were arranged by increasing the values of their real refractive index *n*. The forward design then confirmed the optical absorption spectrum of the simulated multilayer. Moreover, the desired metamaterial was experimentally fabricated on a Si wafer, obtaining 92% average absorptance in the range 400−2500 nm, and its photothermal performance was assessed in outdoor conditions under sunlight, reaching a peak temperature of ~90 °C around midday.

The highly controllable optical properties of metasurfaces present advantages for high-temperature solar-thermal applications, where the radiative losses become more severe (section 2). For example, the TPV technology requires a spectrally selective absorber to harvest concentrated (>100 Suns) solar light to reach high temperatures (1500−2000 K) and a spectrally selective emitter to re-emit such energy matching the bandgap of a PV cell underneath (Figure 11a,b, see also section 2 and Table S5 for additional details). Metasurfaces made of refractory materials can exhibit such high spectral selectivity and withstand repeated thermal cycling and they are often built as in a similar way as MIM multilayers, which are referred to as gap-plasmon metasurfaces.[14,15] For example, a gap-plasmon metasurface consisting of Ti disks/SiO_2/Au layers exhibited >90% absorption in the 900−1825 nm range, which was attributed to the high optical losses of Ti (Figure 11c),[101] whereas a similar structure made of Au disks exhibited a narrowband optical absorption. Metasurfaces based on W nanodisks as solar absorber and thermal emitter for TPV have also been reported (Figure 11d), which could withstand repeated thermal cycling up to 1200 °C in vacuum.[229] By a detailed balance calculation, the predicted TPV efficiency of an integrated absorber/emitter structure could reach 18% at ~1400 °C under 4000 Suns concentration. A remarkable integrated absorber/emitter structure was achieved by patterning the two sides of a Ta plate to realize two photonic crystals (PhCs) with two different absorption/emission spectra (Figure 11e).[230] This was related to the excitation of cavity modes in different spectral regions according to the different geometrical parameters of the PhC. The so-obtained TPV structure was optimized to work at 1300 K and exhibited an efficiency 2.8 times higher than that of a blackbody absorber/emitter system at 130 Suns (Figure 11f). Further studies focusing on TPV applications reported other gap-plasmon metasurfaces, such as based on cross-shaped Cr nanoresonators,[231] metamaterials based on TiN/Si nanopillars,[232] or hybrid metallic/dielectric PhCs.[233]

Most of the aforementioned structures require EBL or complex lithographic fabrication methods and do not offer a high surface area that is available for heterogeneous chemical reactions. The emerging field of photothermal catalysis, on the other hand, can take advantage of the strong photothermal effects produced by metasurfaces under moderate light concentrations (10−20 Suns) achieved by simple concentration optics, to drive industrially relevant chemical reactions in the gas phase, such as using CO_2 as reactant and generating fuels (Figure 12a and Table S6 for additional details).[33,234] As a promising scalable material platform, the self-assembled refractory TiN nanocavities (Figure 10d) were leveraged to realize a photothermal metasurface with catalytic functionality upon decoration with Rh NPs (3−5 nm, Figure 12b).[235] The so-obtained material was tested in the CO oxidation reaction ($2CO + O_2 \rightarrow 2CO_2$) and achieved a rate of CO_2 production of ~16 mol m^{-2} h^{-1} under solar-simulated light intensities >9 Suns (Figure 12c). Furthermore, the sigmoidal shape of the CO_2 generation rate vs light intensity (Figure 12c) highlighted the thermal nature of the catalytic process. A similar thin film system based on TiN nanotubes (~3 μm thick) coated with TiO_2 and In_2O_3 explored the reverse water gas shift reaction ($CO_2 + H_2 \rightarrow CO + H_2O$) under ~10 Suns illumination as a promising route to reduce CO_2 and close the carbon cycle.[236] The role of TiN nanotubes was again to generate heat by thermoplasmonic effects, thus, enhancing the reaction rate. These early results highlighted the potential of plasmonic metasurfaces as alternative systems to standard powdered photocatalysts. Follow-up studies are thus expected in the near future

https://doi.org/10.1021/acsphotonics.3c01013
ACS Photonics XXXX, XXX, XXX−XXX

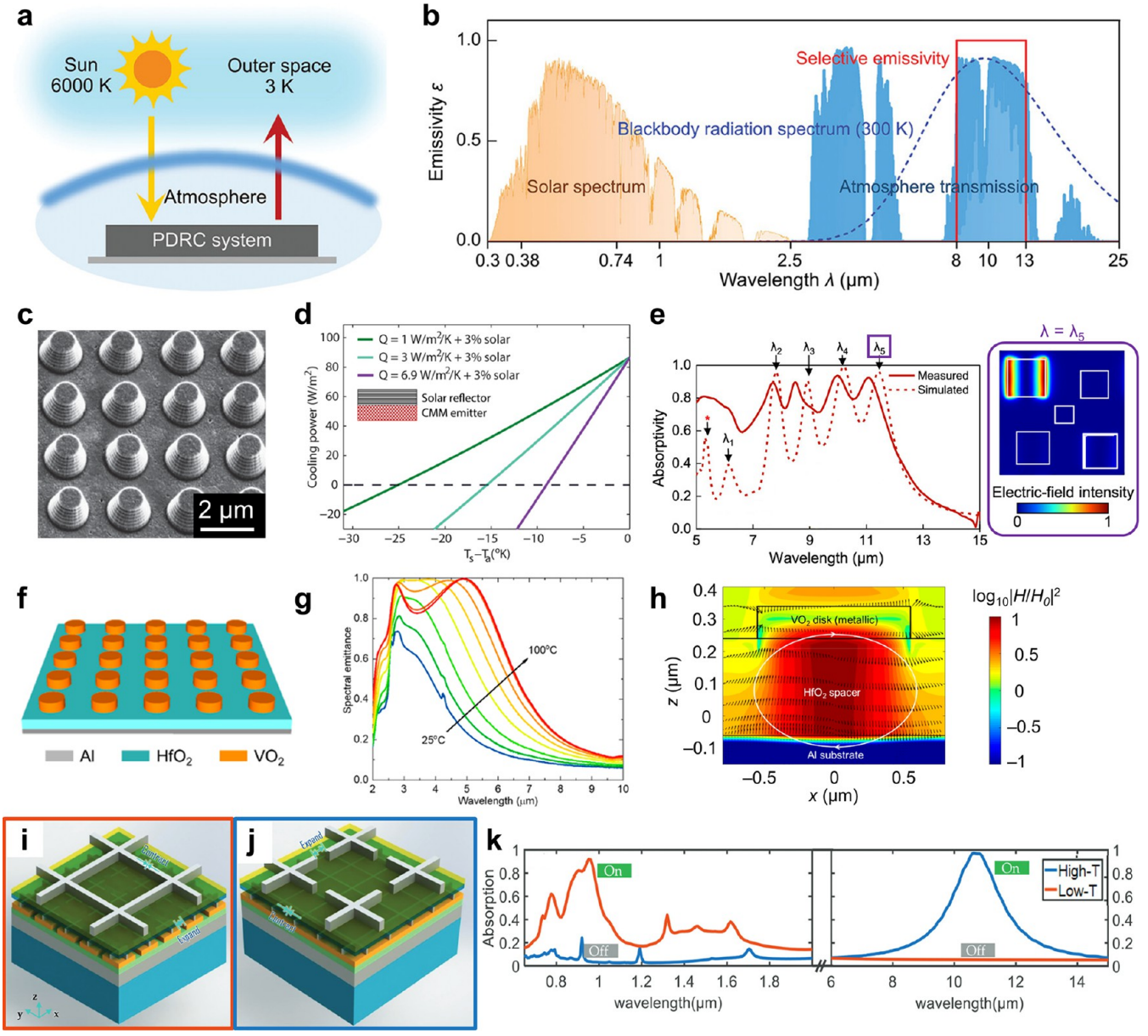

Figure 13. Metasurfaces for radiative cooling. (a) Schematic of passive daytime radiative cooling (PDRC). (b) Optical absorption (or emissivity) spectrum of an ideal PDRC device compared to the blackbody radiation spectrum at 300 K, the AM1.5G solar spectrum and the atmospheric transmission spectrum. (a, b) Reproduced with permission from ref 238. Copyright 2023 Wiley-VCH. (c) Tilted SEM image of a metasurface based on conical multilayer Al−Ge pillars and (d) calculated cooling power of the same with 3% solar absorption and a convective heat exchanger. (c, d) Reproduced with permission from ref 242. Copyright 2015 Wiley-VCH. (e) Optical absorption in Cu/ZnS/Cu multicavity arrays exhibiting five different fundamental gap plasmon cavity modes ($\lambda_1 = 6.2\ \mu m$, $\lambda_2 = 7.8\ \mu m$, $\lambda_3 = 8.9\ \mu m$, $\lambda_4 = 10.2\ \mu m$, $\lambda_5 = 11.6\ \mu m$) and a higher-order mode (* = 5.5 μm). The right panel shows the electric field intensity map along the horizontal plane of the ZnS spacer layer at wavelength $\lambda = \lambda_5$. Adapted with permission from ref 243. Copyright 2021 American Chemical Society. (f) Schematic and (g) spectral emittance at different temperatures (from 25 to 100 °C) of a thermally tunable metasurface based on VO_2 disks deposited on an Al substrate with an HfO_2 spacer. (h) Simulated electromagnetic field distribution at $\lambda = 5\ \mu m$ along the cross section of the VO_2 metasurface in the metallic state. (f–h) Adapted with permission from ref 246. Copyright 2020 American Chemical Society. (i) Schematic of a self-adaptive multilayer metasurface based on "small" and "large" cross resonators at low temperature and (j) at high temperature and (k) corresponding optical absorption spectra. (i–k) Adapted with permission from ref 248. Copyright 2020 Royal Society of Chemistry.

considering the rapid growth of the field of photothermal catalysis.[234,237]

5.4. Metasurfaces for Radiative Cooling. Photothermal effects in metasurfaces can give rise to radiative emission according to the fourth power of the surface temperature. While thermal emission is detrimental to the efficiency of a solar absorber (see section 2), the same phenomenon can be exploited for energy savings purposes by radiative cooling under sunlight illumination, also known as passive daytime radiative cooling (PDRC, Figure 13a and Table S7 for additional details).[49,238] This is based on the radiative heat transfer from an illuminated surface at $T \sim 300$ K to the outer space, which works as an ideal unlimited heat sink at $T \sim 3$ K. The blackbody radiation at 300 K peaks at ~9.6 μm and it matches a transparency window of the Earth's atmosphere (8−13 μm), therefore allowing heat dissipation if the radiating object has a

https://doi.org/10.1021/acsphotonics.3c01013
ACS Photonics XXXX, XXX, XXX−XXX

high emissivity in that spectral range (Figure 13b). More precisely, a radiative cooler needs to dissipate more power by thermal radiation than that absorbed from solar and atmospheric radiation, where the net zero balance must be reached at a temperature $T_{eq} < T_{amb}$. In this way, the radiative cooler can cool an attached material by conduction, as first demonstrated by a planar dielectric photonic structure.[239] In particular, a radiative cooler with negligible solar absorptance, i.e., high transmittance in the 250−2000 nm region of the electromagnetic spectrum, can be placed on top of a solar cell to decrease its temperature by ∼10 °C during operation and, as a consequence, increase its efficiency by ∼1%.[240,241] In this regard, the high optical tunability of metasurfaces represents a key advantage to realize optimized materials for PDRC. For example, a hybrid metal−dielectric structure made of conical multilayer Al−Ge pillars (Figure 13c) was realized by a combination of EBL and electron beam evaporation and exhibited >80% emissivity in the 8−13 μm region.[242] Numerical simulations confirmed that, by coupling such structure with a solar reflector (with 3% absorptance) and realistic values of convective heat exchange (1−6.9 W m^{-2} K^{-1}), it could cool 9 °C below ambient temperature during day-time operation (Figure 13d). An interesting strategy to enhance the MIR emission of a metasurface consisted in the excitation of multiple gap plasmon cavity modes (Figure 13e).[243] The unit cell of a Cu/ZnS/Cu metasurface included five different Cu squares, with sizes ranging from 1.0 to 2.2 μm, on top of the ZnS layer to excite five different gap plasmon cavity modes at increasing wavelengths, ranging from 6.2 to 11.6 μm (Figure 13e, left). For each cavity mode, the electric field was localized at the edges of the cavity, leading to increased optical absorption (see, for example, the mode at $\lambda = \lambda_5$ in Figure 13e, right). At the same time, more than five cavities in the same unit cell did not lead to a performance increase due to near-field coupling between different modes. The Cu/ZnS/Cu gap plasmon metasurfaces were thus tested in outdoor radiative cooling experiments and lowered the temperature of a Si substrate by 4 °C under sunlight illumination (800 mW m^{-2} intensity). Similar results were achieved with a metasurface where the unit cell included two identical rectangular *n*-doped Si resonators coated with Ag orientated orthogonally to each other.[244] Two main resonances were observed at 8.8 and 11.3 μm along the length and width of the rectangular resonators, respectively, which were both assigned to magnetic dipole modes. The use of dielectric metasurfaces was further discussed in a recent example showing a thin transparent multilayer structure made of SiO_2 pillars, acting as MIR emitters, on top of a trilayer ZnO/Ag/ZnO, acting as NIR reflector (with total thickness ∼ 6.6 μm).[245] Such a multilayer exhibited promising cooling performance in a sealed test chamber and may be deposited on flexible substrates. Finally, another interesting approach toward PDRC lies in the exploitation of adaptive or tunable metasurfaces, such as by exploiting the insulator−metal transition of the material constituting the nanoresonators[246,247] or by thermal expansion of a support material.[248] For example, a thermally tunable metasurface based on VO_2 disk resonators deposited on top of HfO_2-coated Al substrate (Figure 13f) exhibited a clear increase in emittance upon heating above the VO_2 transition temperature occurring at ∼60 °C (Figure 13g).[246] The main peak at ∼5 μm was associated with magnetic polariton excitation based on full-wave numerical optical simulations, which showed an electromagnetic energy confinement in the HfO_2 spacer region between the metallic VO_2 disks and the Al substrate together with an electric current loop (Figure 13h). Such a mode was nearly insensitive to the incident excitation angle and could only be observed in metallic VO_2. The thermal expansion approach was instead discussed in a recent numerical study introducing self-adaptive multilayer metasurfaces based on Ag cross resonators of different sizes deposited on polymeric interlayers (Figure 13i and Figure 13j).[248] The optical behavior of the structure shifted from highly absorbing in the solar spectrum region under low ambient temperature, therefore acting as a heating device, to highly emitting in the atmospheric window under high ambient temperature, thus acting as a radiative cooler (Figure 13k). Based on such recent results, further works leveraging deep-learning methods to optimize either passive or active metasurfaces for PDRC are likely expected.[178]

6. CONCLUSIONS AND PERSPECTIVES

The tailorability/tunability of the metasurfaces' optical response has so far been mostly exploited in flat optical devices. More recently, researchers have begun leveraging metasurfaces' properties in solar energy conversion applications, especially broadband optical absorption within a subμm thickness or photoresponse enhancement induced in semiconductors. The most significant breakthroughs in practical applications have been made in the field of thermophotovoltaics with absorber and emitter structures made of refractory metasurfaces. In this case, a relatively expensive fabrication process by EBL is required to achieve a high spectral selectivity, for example, by designing complex unit cells in the resonator array or by combining more materials to realize MIM structures. On the contrary, since photovoltaics has already reached commercial maturity, it poses more strict requirements on the fabrication cost to justify the usage of metasurfaces. The same argument applies to photocatalysis and photoelectrochemistry, which do not require a high performance under extreme temperature conditions but rather a high scalability potential. Photothermal catalysis lies in between, as it requires high stability under repeated thermal cycling to activate gas-phase catalytic processes but, simultaneously, a low fabrication cost. The latter would have a crucial role in enabling decentralized reactors to work under moderate light concentrations as opposed to large industrial infrastructures currently used for thermal catalysis (i.e., ammonia synthesis and Fischer−Tropsch chemistry). The possibility of employing metasurfaces enclosed in flat panel-like reactors working at low concentration factors to drive industrially relevant chemical reactions is undoubtedly a very appealing feature, which will likely lead to remarkable progress of this research field.

The promising results obtained so far show a great promise of practical metasurface applications in solar energy conversion processes. Since decentralized reactors require scalable fabrication methods and materials, metasurfaces can be fabricated using large-scale, CMOS-compatible nanoimprint lithography and photolithography. In regard to low-cost, abundant materials, there is a rising interest in transition metal nitrides for plasmonic metasurfaces and doped metal oxides for dielectric metasurfaces. For example, nanotube arrays made of titanium oxides or nitrides may be further investigated in photothermal catalysis applications because they combine an industrially friendly fabrication process (i.e., anodization followed by thermal treatments) with a long-range order. These materials are also CMOS-compatible, high-temperature- and chemically stable, and offer a high surface area, which is a key requirement of materials involved in chemical reactions. Therefore, Ti-based metasurfaces appear as promising candi-

https://doi.org/10.1021/acsphotonics.3c01013
ACS Photonics XXXX, XXX, XXX−XXX

dates for a wide range of photocatalytic, photoelectrochemical, and photothermal processes.

So far, the role of advanced numerical simulations in the design of efficient metasurfaces has not yet been fully explored for solar energy conversion applications. Numerical methods could be more systematically used to design metasurfaces exhibiting the required optical absorption depending on their specific role in the energy-conversion device and therefore guide the experiments, avoiding typical trial-and-error approaches. Examples include designs of a spectrally selective absorber for metasurfaces in TPV and photothermal catalysis, where complex unit cell geometries are obtained by an inverse design approach. Numerical methods could also guide the design of more advanced metasurfaces (e.g., chiral), enabling a deeper understanding of thermal and electronic effects under solar light illumination.

Practical implementation of metasurfaces in solar energy conversion devices requires more systematic studies focusing on benchmarking and estimating the efficiency in a specific field of application. Contrary to the well-established efficiency metrics that are routinely reported in photovoltaics, the fields of photocatalysis, photoelectrochemistry, and especially photothermal catalysis have not yet standardized according to univocal protocols. This is due to an intrinsic higher number of experimental parameters involved in such experiments and to the wide variety of chemical reactions involved, including spontaneous and nonspontaneous processes. For example, by comparing Tables S6 and S8, which report examples of metasurfaces and powdered plasmonic systems for photothermal catalysis, respectively, one can note a great variety of experimental conditions, including the light source and the definition of the reaction rate, which prevent a straightforward comparison and definition of univocal performance metrics. In the specific case of photothermal catalysis, moreover, such issues are further exacerbated by the early stage of this research field and by the intricated disentangling of thermal from nonthermal effects, which requires dedicated experimental procedures.

Designing future generations of metasurfaces for solar energy conversion would therefore seamlessly combine the performance requirements set by the targeted application, advanced numerical and machine-learning-assisted approaches, low-cost, scalable manufacturing involving Earth-abundant materials, as well as appropriate performance, durability, and cost benchmarking.

■ ASSOCIATED CONTENT

Supporting Information

The Supporting Information is available free of charge at https://pubs.acs.org/doi/10.1021/acsphotonics.3c01013.

Performance tables for metasurfaces for photovoltaics, catalytic processes, solar-thermal processes, and radiative cooling; additional performance table for plasmonic nanomaterials for gas-phase photothermal catalysis (PDF)

■ AUTHOR INFORMATION

Corresponding Authors

Alberto Naldoni − *Department of Chemistry and NIS Centre, University of Turin, Turin 10125, Italy;* orcid.org/0000-0001-5932-2125; Email: alberto.naldoni@unito.it

Alexandra Boltasseva − *Elmore Family School of Electrical and Computer Engineering, Birck Nanotechnology Center, and Purdue Quantum Science and Engineering Institute, Purdue University, West Lafayette, Indiana 47907, United States; The Quantum Science Center (QSC), a National Quantum Information Science Research Center of the U.S. Department of Energy (DOE), Oak Ridge, Tennessee 37931, United States;* orcid.org/0000-0001-8905-2605; Email: aeb@purdue.edu

Authors

Luca Mascaretti − *Czech Advanced Technology and Research Institute, Regional Centre of Advanced Technologies and Materials, Palacký University Olomouc, 77900 Olomouc, Czech Republic; Department of Physical Electronics, Faculty of Nuclear Sciences and Physical Engineering, Czech Technical University in Prague, 11519 Prague, Czech Republic;* orcid.org/0000-0001-8997-7018

Yuheng Chen − *Elmore Family School of Electrical and Computer Engineering, Birck Nanotechnology Center, and Purdue Quantum Science and Engineering Institute, Purdue University, West Lafayette, Indiana 47907, United States; The Quantum Science Center (QSC), a National Quantum Information Science Research Center of the U.S. Department of Energy (DOE), Oak Ridge, Tennessee 37931, United States*

Olivier Henrotte − *Czech Advanced Technology and Research Institute, Regional Centre of Advanced Technologies and Materials, Palacký University Olomouc, 77900 Olomouc, Czech Republic;* orcid.org/0000-0002-7512-3377

Omer Yesilyurt − *Elmore Family School of Electrical and Computer Engineering, Birck Nanotechnology Center, and Purdue Quantum Science and Engineering Institute, Purdue University, West Lafayette, Indiana 47907, United States; The Quantum Science Center (QSC), a National Quantum Information Science Research Center of the U.S. Department of Energy (DOE), Oak Ridge, Tennessee 37931, United States;* orcid.org/0000-0002-9829-5219

Vladimir M. Shalaev − *Elmore Family School of Electrical and Computer Engineering, Birck Nanotechnology Center, and Purdue Quantum Science and Engineering Institute, Purdue University, West Lafayette, Indiana 47907, United States; The Quantum Science Center (QSC), a National Quantum Information Science Research Center of the U.S. Department of Energy (DOE), Oak Ridge, Tennessee 37931, United States*

Complete contact information is available at: https://pubs.acs.org/10.1021/acsphotonics.3c01013

Funding

L.M. and O.H. gratefully acknowledge the support from the funding from Czech Science Foundation (GACR) through the Project 22-26416S. L.M. further acknowledges the support from Ministry of Education, Youth, and Sports of the Czech Republic, CAAS - Project Center of Advanced Applied Sciences, Project Number: CZ.02.1.01/0.0/0.0/16 019/0000778 (European Structural and Investments Funds, Operational Programme Research, Development, and Education). A.N. acknowledges the support from the Project CH4.0 under the MIUR program "Dipartimenti di Eccellenza 2023-2027" (CUP: D13C2200352001). Y.C., O.Y., V.M.S., and A.B. acknowledge the Air Force Office of Scientific Research (AFOSR) under Award FA9550-20-1-0124, the National Science Foundation (NSF) under Award 2029553-ECCS, and the Purdue ECE Elmore Emerging Frontiers Center "The Crossroads of Quantum and AI".

Notes

The authors declare no competing financial interest.

REFERENCES

(1) IRENA. World Energy Transitions Outlook: 1.5°C Pathway, 2022. https://www.irena.org/publications/2022/Mar/World-Energy-Transitions-Outlook-2022 (accessed 2022−04−08).

(2) Paris Agreement | UNFCCC. https://unfccc.int/process-and-meetings/the-paris-agreement/the-paris-agreement (accessed 2022−02−15).

(3) Lewis, N. S.; Crabtree, G. Basic Research Needs for Solar Energy Utilization: Report of the Basic Energy Sciences Workshop on Solar Energy Utilization, April 18−21, 2005; US Department of Energy, Office of Basic Energy Science: Washington, DC, 2005. http://authors.library.caltech.edu/8599/.

(4) Key World Energy Statistics 2021. https://www.iea.org/reports/key-world-energy-statistics-2021 (accessed 2022−01−18).

(5) Quevedo-Teruel, O.; Chen, H.; Díaz-Rubio, A.; Gok, G.; Grbic, A.; Minatti, G.; Martini, E.; Maci, S.; Eleftheriades, G. V.; Chen, M.; Zheludev, N. I.; Papasimakis, N.; Choudhury, S.; Kudyshev, Z. A.; Saha, S.; Reddy, H.; Boltasseva, A.; Shalaev, V. M.; Kildishev, A. V.; Sievenpiper, D.; Caloz, C.; Alù, A.; He, Q.; Zhou, L.; Valerio, G.; Rajo-Iglesias, E.; Sipus, Z.; Mesa, F.; Rodríguez-Berral, R.; Medina, F.; Asadchy, V.; Tretyakov, S.; Craeye, C. Roadmap on Metasurfaces. *J. Opt.* **2019**, *21* (7), 073002.

(6) Genevet, P.; Capasso, F.; Aieta, F.; Khorasaninejad, M.; Devlin, R. Recent Advances in Planar Optics: From Plasmonic to Dielectric Metasurfaces. *Optica* **2017**, *4* (1), 139−152.

(7) Khorasaninejad, M.; Capasso, F. Metalenses: Versatile Multifunctional Photonic Components. *Science* **2017**, *358* (6367), No. eaam8100.

(8) Li, Z.; Pestourie, R.; Lin, Z.; Johnson, S. G.; Capasso, F. Empowering Metasurfaces with Inverse Design: Principles and Applications. *ACS Photonics* **2022**, *9* (7), 2178−2192.

(9) Yu, N.; Capasso, F. Flat Optics with Designer Metasurfaces. *Nat. Mater.* **2014**, *13* (2), 139−150.

(10) Chen, W. T.; Zhu, A. Y.; Capasso, F. Flat Optics with Dispersion-Engineered Metasurfaces. *Nat. Rev. Mater.* **2020**, *5* (8), 604−620.

(11) Lin, D.; Fan, P.; Hasman, E.; Brongersma, M. L. Dielectric Gradient Metasurface Optical Elements. *Science* **2014**, *345* (6194), 298−302.

(12) Kuznetsov, A. I.; Miroshnichenko, A. E.; Brongersma, M. L.; Kivshar, Y. S.; Luk'yanchuk, B. Optically Resonant Dielectric Nanostructures. *Science* **2016**, *354* (6314), aag2472.

(13) Lalanne, P.; Chavel, P. Metalenses at Visible Wavelengths: Past, Present, Perspectives. *Laser Photonics Rev.* **2017**, *11* (3), 1600295.

(14) Hsiao, H.-H.; Chu, C. H.; Tsai, D. P. Fundamentals and Applications of Metasurfaces. *Small Methods* **2017**, *1* (4), 1600064.

(15) Ding, F.; Yang, Y.; Deshpande, R. A.; Bozhevolnyi, S. I. A Review of Gap-Surface Plasmon Metasurfaces: Fundamentals and Applications. *Nanophotonics* **2018**, *7* (6), 1129−1156.

(16) Krasnok, A.; Tymchenko, M.; Alù, A. Nonlinear Metasurfaces: A Paradigm Shift in Nonlinear Optics. *Mater. Today* **2018**, *21* (1), 8−21.

(17) Solntsev, A. S.; Agarwal, G. S.; Kivshar, Y. S. Metasurfaces for Quantum Photonics. *Nat. Photonics* **2021**, *15* (5), 327−336.

(18) Su, V.-C.; Chu, C. H.; Sun, G.; Tsai, D. P. Advances in Optical Metasurfaces: Fabrication and Applications [Invited]. *Opt. Express* **2018**, *26* (10), 13148−13182.

(19) Deng, Y.; Cai, Z.; Ding, Y.; Bozhevolnyi, S. I.; Ding, F. Recent Progress in Metasurface-Enabled Optical Waveplates. *Nanophotonics* **2022**, *11* (10), 2219−2244.

(20) Overvig, A. C.; Malek, S. C.; Yu, N. Multifunctional Nonlocal Metasurfaces. *Phys. Rev. Lett.* **2020**, *125* (1), 017402.

(21) Shirmanesh, G. K.; Sokhoyan, R.; Wu, P. C.; Atwater, H. A. Electro-Optically Tunable Multifunctional Metasurfaces. *ACS Nano* **2020**, *14* (6), 6912−6920.

(22) Kwon, H.; Sounas, D.; Cordaro, A.; Polman, A.; Alù, A. Nonlocal Metasurfaces for Optical Signal Processing. *Phys. Rev. Lett.* **2018**, *121* (17), 173004.

(23) Qiu, C.-W.; Zhang, T.; Hu, G.; Kivshar, Y. Quo Vadis, Metasurfaces? *Nano Lett.* **2021**, *21* (13), 5461−5474.

(24) Chen, H.-T.; Taylor, A. J.; Yu, N. A Review of Metasurfaces: Physics and Applications. *Rep. Prog. Phys.* **2016**, *79* (7), 076401.

(25) Minovich, A. E.; Miroshnichenko, A. E.; Bykov, A. Y.; Murzina, T. V.; Neshev, D. N.; Kivshar, Y. S. Functional and Nonlinear Optical Metasurfaces. *Laser Photonics Rev.* **2015**, *9* (2), 195−213.

(26) Glybovski, S. B.; Tretyakov, S. A.; Belov, P. A.; Kivshar, Y. S.; Simovski, C. R. Metasurfaces: From Microwaves to Visible. *Phys. Rep.* **2016**, *634*, 1−72.

(27) Yu, N.; Genevet, P.; Kats, M. A.; Aieta, F.; Tetienne, J.-P.; Capasso, F.; Gaburro, Z. Light Propagation with Phase Discontinuities: Generalized Laws of Reflection and Refraction. *Science* **2011**, *334* (6054), 333−337.

(28) Aieta, F.; Genevet, P.; Yu, N.; Kats, M. A.; Gaburro, Z.; Capasso, F. Out-of-Plane Reflection and Refraction of Light by Anisotropic Optical Antenna Metasurfaces with Phase Discontinuities. *Nano Lett.* **2012**, *12* (3), 1702−1706.

(29) Shalaev, V. M.; Cai, W.; Chettiar, U. K.; Yuan, H.-K.; Sarychev, A. K.; Drachev, V. P.; Kildishev, A. V. Negative Index of Refraction in Optical Metamaterials. *Opt. Lett.* **2005**, *30* (24), 3356−3358.

(30) Zheludev, N. I.; Kivshar, Y. S. From Metamaterials to Metadevices. *Nat. Mater.* **2012**, *11* (11), 917−924.

(31) Shaltout, A. M.; Shalaev, V. M.; Brongersma, M. L. Spatiotemporal Light Control with Active Metasurfaces. *Science* **2019**, *364* (6441), 648.

(32) Cortés, E.; Wendisch, F. J.; Sortino, L.; Mancini, A.; Ezendam, S.; Saris, S.; de S. Menezes, L.; Tittl, A.; Ren, H.; Maier, S. A. Optical Metasurfaces for Energy Conversion. *Chem. Rev.* **2022**, *122* (19), 15082−15176.

(33) Mascaretti, L.; Schirato, A.; Fornasiero, P.; Boltasseva, A.; Shalaev, V. M.; Alabastri, A.; Naldoni, A. Challenges and Prospects of Plasmonic Metasurfaces for Photothermal Catalysis. *Nanophotonics* **2022**, *11* (13), 3035−3056.

(34) Yu, M.-J.; Chang, C.-L.; Lan, H.-Y.; Chiao, Z.-Y.; Chen, Y.-C.; Howard Lee, H. W.; Chang, Y.-C.; Chang, S.-W.; Tanaka, T.; Tung, V.; Chou, H.-H.; Lu, Y.-J. Plasmon-Enhanced Solar-Driven Hydrogen Evolution Using Titanium Nitride Metasurface Broadband Absorbers. *ACS Photonics* **2021**, *8* (11), 3125−3132.

(35) Hüttenhofer, L.; Golibrzuch, M.; Bienek, O.; Wendisch, F. J.; Lin, R.; Becherer, M.; Sharp, I. D.; Maier, S. A.; Cortés, E. Metasurface Photoelectrodes for Enhanced Solar Fuel Generation. *Adv. Energy Mater.* **2021**, *11* (46), 2102877.

(36) Li, N.; Xu, Z.; Dong, Y.; Hu, T.; Zhong, Q.; Fu, Y. H.; Zhu, S.; Singh, N. Large-Area Metasurface on CMOS-Compatible Fabrication Platform: Driving Flat Optics from Lab to Fab. *Nanophotonics* **2020**, *9* (10), 3071−3087.

(37) Chang, S.; Guo, X.; Ni, X. Optical Metasurfaces: Progress and Applications. *Annu. Rev. Mater. Res.* **2018**, *48* (1), 279−302.

(38) Liu, G.-X.; Liu, J.-F.; Zhou, W.-J.; Li, L.-Y.; You, C.-L.; Qiu, C.-W.; Wu, L. Inverse Design in Quantum Nanophotonics: Combining Local-Density-of-States and Deep Learning. *Nanophotonics* **2023**, *12* (11), 1943−1955.

(39) Liu, Z.; Zhu, D.; Rodrigues, S. P.; Lee, K.-T.; Cai, W. Generative Model for the Inverse Design of Metasurfaces. *Nano Lett.* **2018**, *18* (10), 6570−6576.

(40) So, S.; Badloe, T.; Noh, J.; Bravo-Abad, J.; Rho, J. Deep Learning Enabled Inverse Design in Nanophotonics. *Nanophotonics* **2020**, *9* (5), 1041−1057.

(41) Jiang, J.; Fan, J. A. Simulator-Based Training of Generative Neural Networks for the Inverse Design of Metasurfaces. *Nanophotonics* **2020**, *9* (5), 1059−1069.

(42) Haegel, N. M.; Verlinden, P.; Victoria, M.; Altermatt, P.; Atwater, H.; Barnes, T.; Breyer, C.; Case, C.; De Wolf, S.; Deline, C.; Dharmrin, M.; Dimmler, B.; Gloeckler, M.; Goldschmidt, J. C.; Hallam, B.; Haussener, S.; Holder, B.; Jaeger, U.; Jaeger-Waldau, A.; Kaizuka, I.; Kikusato, H.; Kroposki, B.; Kurtz, S.; Matsubara, K.; Nowak, S.; Ogimoto, K.; Peter, C.; Peters, I. M.; Philipps, S.; Powalla, M.; Rau, U.; Reindl, T.; Roumpani, M.; Sakurai, K.; Schorn, C.; Schossig, P.;

https://doi.org/10.1021/acsphotonics.3c01013
ACS Photonics XXXX, XXX, XXX−XXX

Schlatmann, R.; Sinton, R.; Slaoui, A.; Smith, B. L.; Schneidewind, P.; Stanbery, B.; Topic, M.; Tumas, W.; Vasi, J.; Vetter, M.; Weber, E.; Weeber, A. W.; Weidlich, A.; Weiss, D.; Bett, A. W. Photovoltaics at Multi-Terawatt Scale: Waiting Is Not an Option. *Science* **2023**, *380* (6640), 39−42.
(43) Ballif, C.; Haug, F.-J.; Boccard, M.; Verlinden, P. J.; Hahn, G. Status and Perspectives of Crystalline Silicon Photovoltaics in Research and Industry. *Nat. Rev. Mater.* **2022**, *7* (8), 597−616.
(44) Duan, L.; Walter, D.; Chang, N.; Bullock, J.; Kang, D.; Phang, S. P.; Weber, K.; White, T.; Macdonald, D.; Catchpole, K.; Shen, H. Stability Challenges for the Commercialization of Perovskite-Silicon Tandem Solar Cells. *Nat. Rev. Mater.* **2023**, *8* (4), 261−281.
(45) Green, M. A.; Dunlop, E. D.; Yoshita, M.; Kopidakis, N.; Bothe, K.; Siefer, G.; Hao, X. Solar Cell Efficiency Tables (Version 62). *Prog. Photovolt. Res. Appl.* **2023**, *31* (7), 651−663.
(46) Almora, O.; Baran, D.; Bazan, G. C.; Cabrera, C. I.; Erten-Ela, S.; Forberich, K.; Guo, F.; Hauch, J.; Ho-Baillie, A. W. Y.; Jacobsson, T. J.; Janssen, R. A. J.; Kirchartz, T.; Kopidakis, N.; Loi, M. A.; Lunt, R. R.; Mathew, X.; McGehee, M. D.; Min, J.; Mitzi, D. B.; Nazeeruddin, M. K.; Nelson, J.; Nogueira, A. F.; Paetzold, U. W.; Rand, B. P.; Rau, U.; Snaith, H. J.; Unger, E.; Vaillant-Roca, L.; Yang, C.; Yip, H.-L.; Brabec, C. J. Device Performance of Emerging Photovoltaic Materials (Version 3). *Adv. Energy Mater.* **2023**, *13* (1), 2203313.
(47) Weinstein, L. A.; Loomis, J.; Bhatia, B.; Bierman, D. M.; Wang, E. N.; Chen, G. Concentrating Solar Power. *Chem. Rev.* **2015**, *115* (23), 12797−12838.
(48) Saidur, R.; Elcevvadi, E. T.; Mekhilef, S.; Safari, A.; Mohammed, H. A. An Overview of Different Distillation Methods for Small Scale Applications. *Renew. Sustain. Energy Rev.* **2011**, *15* (9), 4756−4764.
(49) Li, W.; Fan, S. Nanophotonic Control of Thermal Radiation for Energy Applications [Invited]. *Opt. Express* **2018**, *26* (12), 15995−16021.
(50) Wang, Q.; Domen, K. Particulate Photocatalysts for Light-Driven Water Splitting: Mechanisms, Challenges, and Design Strategies. *Chem. Rev.* **2020**, *120* (2), 919−985.
(51) Melchionna, M.; Fornasiero, P. Updates on the Roadmap for Photocatalysis. *ACS Catal.* **2020**, *10*, 5493−5501.
(52) Segev, G.; Kibsgaard, J.; Hahn, C.; Xu, Z. J.; Cheng, W.-H. S.; Deutsch, T. G.; Xiang, C.; Zhang, J. Z.; Hammarström, L.; Nocera, D. G.; Weber, A. Z.; Agbo, P.; Hisatomi, T.; Osterloh, F. E.; Domen, K.; Abdi, F. F.; Haussener, S.; Miller, D. J.; Ardo, S.; McIntyre, P. C.; Hannappel, T.; Hu, S.; Atwater, H.; Gregoire, J. M.; Ertem, M. Z.; Sharp, I. D.; Choi, K.-S.; Lee, J. S.; Ishitani, O.; Ager, J. W.; Prabhakar, R. R.; Bell, A. T.; Boettcher, S. W.; Vincent, K.; Takanabe, K.; Artero, V.; Napier, R.; Cuenya, B. R.; Koper, M. T. M.; Van de Krol, R.; Houle, F. The 2022 Solar Fuels Roadmap. *J. Phys. Appl. Phys.* **2022**, *55* (32), 323003.
(53) Sivula, K.; van de Krol, R. Semiconducting Materials for Photoelectrochemical Energy Conversion. *Nat. Rev. Mater.* **2016**, *1*, 15010.
(54) Romano, V.; D'Angelo, G.; Perathoner, S.; Centi, G. Current Density in Solar Fuel Technologies. *Energy Environ. Sci.* **2021**, *14* (11), 5760−5787.
(55) Spitler, M. T.; Modestino, M. A.; Deutsch, T. G.; Xiang, C. X.; Durrant, J. R.; Esposito, D. V.; Haussener, S.; Maldonado, S.; Sharp, I. D.; Parkinson, B. A.; Ginley, D. S.; Houle, F. A.; Hannappel, T.; Neale, N. R.; Nocera, D. G.; McIntyre, P. C. Practical Challenges in the Development of Photoelectrochemical Solar Fuels Production. *Sustain. Energy Fuels* **2020**, *4* (3), 985−995.
(56) Carrillo, A. J.; González-Aguilar, J.; Romero, M.; Coronado, J. M. Solar Energy on Demand: A Review on High Temperature Thermochemical Heat Storage Systems and Materials. *Chem. Rev.* **2019**, *119* (7), 4777−4816.
(57) Zhou, Z.; Sakr, E.; Sun, Y.; Bermel, P. Solar Thermophotovoltaics: Reshaping the Solar Spectrum. *Nanophotonics* **2016**, *5* (1), 1−21.
(58) Burger, T.; Sempere, C.; Roy-Layinde, B.; Lenert, A. Present Efficiencies and Future Opportunities in Thermophotovoltaics. *Joule* **2020**, *4* (8), 1660−1680.
(59) Ghoussoub, M.; Xia, M.; Duchesne, P. N.; Segal, D.; Ozin, G. Principles of Photothermal Gas-Phase Heterogeneous CO2 Catalysis. *Energy Environ. Sci.* **2019**, *12* (4), 1122−1142.
(60) Mascaretti, L.; Schirato, A.; Montini, T.; Alabastri, A.; Naldoni, A.; Fornasiero, P. Challenges in Temperature Measurements in Gas-Phase Photothermal Catalysis. *Joule* **2022**, *6* (8), 1727−1732.
(61) Ra'di, Y.; Simovski, C. R.; Tretyakov, S. A. Thin Perfect Absorbers for Electromagnetic Waves: Theory, Design, and Realizations. *Phys. Rev. Appl.* **2015**, *3* (3), 037001.
(62) Tagliabue, G.; Eghlidi, H.; Poulikakos, D. Rapid-Response Low Infrared Emission Broadband Ultrathin Plasmonic Light Absorber. *Sci. Rep.* **2014**, *4*, 7181.
(63) Yang, K.; Wang, J.; Yao, X.; Lyu, D.; Zhu, J.; Yang, Z.; Liu, B.; Ren, B. Large-Area Plasmonic Metamaterial with Thickness-Dependent Absorption. *Adv. Opt. Mater.* **2021**, *9* (1), 2001375.
(64) Patsalas, P.; Kalfagiannis, N.; Kassavetis, S.; Abadias, G.; Bellas, D. V.; Lekka, Ch.; Lidorikis, E. Conductive Nitrides: Growth Principles, Optical and Electronic Properties, and Their Perspectives in Photonics and Plasmonics. *Mater. Sci. Eng. R Rep.* **2018**, *123*, 1−55.
(65) Gui, L.; Bagheri, S.; Strohfeldt, N.; Hentschel, M.; Zgrabik, C. M.; Metzger, B.; Linnenbank, H.; Hu, E. L.; Giessen, H. Nonlinear Refractory Plasmonics with Titanium Nitride Nanoantennas. *Nano Lett.* **2016**, *16* (9), 5708−5713.
(66) Gadalla, M. N.; Chaudhary, K.; Zgrabik, C. M.; Capasso, F.; Hu, E. L. Imaging of Surface Plasmon Polaritons in Low-Loss Highly Metallic Titanium Nitride Thin Films in Visible and Infrared Regimes. *Opt. Express* **2020**, *28* (10), 14536−14546.
(67) Ishii, S.; Shinde, S. L.; Jevasuwan, W.; Fukata, N.; Nagao, T. Hot Electron Excitation from Titanium Nitride Using Visible Light. *ACS Photonics* **2016**, *3* (9), 1552−1557.
(68) Ishii, S.; Higashino, M.; Goya, S.; Shkondin, E.; Tanaka, K.; Nagao, T.; Takayama, O.; Murai, S. Extreme Thermal Anisotropy in High-Aspect-Ratio Titanium Nitride Nanostructures for Efficient Photothermal Heating. *Nanophotonics* **2021**, *10* (5), 1487−1494.
(69) Wang, Y.; Capretti, A.; Dal Negro, L. Wide Tuning of the Optical and Structural Properties of Alternative Plasmonic Materials. *Opt. Mater. Express* **2015**, *5* (11), 2415−2430.
(70) Briggs, J. A.; Naik, G. V.; Petach, T. A.; Baum, B. K.; Goldhaber-Gordon, D.; Dionne, J. A. Fully CMOS-Compatible Titanium Nitride Nanoantennas. *Appl. Phys. Lett.* **2016**, *108* (5), 051110.
(71) Krekeler, T.; Rout, S. S.; Krishnamurthy, G. V.; Störmer, M.; Arya, M.; Ganguly, A.; Sutherland, D. S.; Bozhevolnyi, S. I.; Ritter, M.; Pedersen, K.; Petrov, A. Y.; Eich, M.; Chirumamilla, M. Unprecedented Thermal Stability of Plasmonic Titanium Nitride Films up to 1400 °C. *Adv. Opt. Mater.* **2021**, *9* (16), 2100323.
(72) Chang, C.-C.; Kuo, S.-C.; Cheng, H.-E.; Chen, H.-T.; Yang, Z.-P. Broadband Titanium Nitride Disordered Metasurface Absorbers. *Opt. Express* **2021**, *29* (26), 42813−42826.
(73) Naik, G. V.; Shalaev, V. M.; Boltasseva, A. Alternative Plasmonic Materials: Beyond Gold and Silver. *Adv. Mater.* **2013**, *25* (24), 3264−3294.
(74) Jaffray, W.; Saha, S.; Shalaev, V. M.; Boltasseva, A.; Ferrera, M. Transparent Conducting Oxides: From All-Dielectric Plasmonics to a New Paradigm in Integrated Photonics. *Adv. Opt. Photonics* **2022**, *14* (2), 148−208.
(75) Fujishima, A.; Zhang, X.; Tryk, D. A. TiO2 Photocatalysis and Related Surface Phenomena. *Surf. Sci. Rep.* **2008**, *63* (12), 515−582.
(76) Etacheri, V.; Di Valentin, C.; Schneider, J.; Bahnemann, D.; Pillai, S. C. Visible-Light Activation of TiO2 Photocatalysts: Advances in Theory and Experiments. *J. Photochem. Photobiol. C Photochem. Rev.* **2015**, *25*, 1−29.
(77) Look, D. C.; Leach, J. H. On the Accurate Determination of Absorption Coefficient from Reflectanceand Transmittance Measurements: Application to Fe-Doped GaN. *J. Vac. Sci. Technol. B* **2016**, *34* (4), 04J105.
(78) Langereis, E.; Heil, S. B. S.; Knoops, H. C. M.; Keuning, W.; van de Sanden, M. C. M.; Kessels, W. M. M. In Situ Spectroscopic Ellipsometry as a Versatile Tool for Studying Atomic Layer Deposition. *J. Phys. Appl. Phys.* **2009**, *42* (7), 073001.

https://doi.org/10.1021/acsphotonics.3c01013
ACS Photonics XXXX, XXX, XXX−XXX

(79) Kim, J.; Naik, G. V.; Emani, N. K.; Guler, U.; Boltasseva, A. Plasmonic Resonances in Nanostructured Transparent Conducting Oxide Films. *IEEE J. Sel. Top. Quantum Electron.* **2013**, *19* (3), 4601907−4601907.
(80) Jolivet, A.; Labbé, C.; Frilay, C.; Debieu, O.; Marie, P.; Horcholle, B.; Lemarié, F.; Portier, X.; Grygiel, C.; Duprey, S.; Jadwisienczak, W.; Ingram, D.; Upadhyay, M.; David, A.; Fouchet, A.; Lüders, U.; Cardin, J. Structural, Optical, and Electrical Properties of TiO2 Thin Films Deposited by ALD: Impact of the Substrate, the Deposited Thickness and the Deposition Temperature. *Appl. Surf. Sci.* **2023**, *608*, 155214.
(81) Alaee, R.; Rockstuhl, C.; Fernandez-Corbaton, I. Exact Multipolar Decompositions with Applications in Nanophotonics. *Adv. Opt. Mater.* **2019**, *7* (1), 1800783.
(82) Riccardi, M.; Kiselev, A.; Achouri, K.; Martin, O. J. F. Multipolar Expansions for Scattering and Optical Force Calculations beyond the Long Wavelength Approximation. *Phys. Rev. B* **2022**, *106* (11), 115428.
(83) Maier, S. A. *Plasmonics: Fundamentals and Applications*; Springer Science & Business Media, 2007.
(84) Kravets, V. G.; Kabashin, A. V.; Barnes, W. L.; Grigorenko, A. N. Plasmonic Surface Lattice Resonances: A Review of Properties and Applications. *Chem. Rev.* **2018**, *118* (12), 5912−5951.
(85) Schirato, A.; Maiuri, M.; Cerullo, G.; Della Valle, G. Ultrafast Hot Electron Dynamics in Plasmonic Nanostructures: Experiments, Modelling, Design. *Nanophotonics* **2023**, *12* (1), 1−28.
(86) Besteiro, L. V.; Yu, P.; Wang, Z.; Holleitner, A. W.; Hartland, G. V.; Wiederrecht, G. P.; Govorov, A. O. The Fast and the Furious: Ultrafast Hot Electrons in Plasmonic Metastructures. Size and Structure Matter. *Nano Today* **2019**, *27*, 120−145.
(87) Erwin, W. R.; Zarick, H. F.; Talbert, E. M.; Bardhan, R. Light Trapping in Mesoporous Solar Cells with Plasmonic Nanostructures. *Energy Environ. Sci.* **2016**, *9* (5), 1577−1601.
(88) Yuan, L.; Bourgeois, B. B.; Carlin, C. C.; da Jornada, F. H.; Dionne, J. A. Sustainable Chemistry with Plasmonic Photocatalysts. *Nanophotonics* **2023**, *12* (14), 2745−2762.
(89) Zhang, Y.; Guo, W.; Zhang, Y.; Wei, W. D. Plasmonic Photoelectrochemistry: In View of Hot Carriers. *Adv. Mater.* **2021**, *33* (46), 2006654.
(90) Zhou, L.; Swearer, D. F.; Zhang, C.; Robatjazi, H.; Zhao, H.; Henderson, L.; Dong, L.; Christopher, P.; Carter, E. A.; Nordlander, P.; Halas, N. J. Quantifying Hot Carrier and Thermal Contributions in Plasmonic Photocatalysis. *Science* **2018**, *362* (6410), 69−72.
(91) Zhou, L.; Martirez, J. M. P.; Finzel, J.; Zhang, C.; Swearer, D. F.; Tian, S.; Robatjazi, H.; Lou, M.; Dong, L.; Henderson, L.; Christopher, P.; Carter, E. A.; Nordlander, P.; Halas, N. J. Light-Driven Methane Dry Reforming with Single Atomic Site Antenna-Reactor Plasmonic Photocatalysts. *Nat. Energy* **2020**, *5*, 61−70.
(92) Brown, A. M.; Sundararaman, R.; Narang, P.; Goddard, W. A.; Atwater, H. A. Nonradiative Plasmon Decay and Hot Carrier Dynamics: Effects of Phonons, Surfaces, and Geometry. *ACS Nano* **2016**, *10* (1), 957−966.
(93) Habib, A.; Florio, F.; Sundararaman, R. Hot Carrier Dynamics in Plasmonic Transition Metal Nitrides. *J. Opt.* **2018**, *20* (6), 064001.
(94) Baffou, G.; Quidant, R.; Girard, C. Heat Generation in Plasmonic Nanostructures: Influence of Morphology. *Appl. Phys. Lett.* **2009**, *94* (15), 153109.
(95) Baffou, G.; Berto, P.; Bermúdez Ureña, E.; Quidant, R.; Monneret, S.; Polleux, J.; Rigneault, H. Photoinduced Heating of Nanoparticle Arrays. *ACS Nano* **2013**, *7* (8), 6478−6488.
(96) Richardson, H. H.; Carlson, M. T.; Tandler, P. J.; Hernandez, P.; Govorov, A. O. Experimental and Theoretical Studies of Light-to-Heat Conversion and Collective Heating Effects in Metal Nanoparticle Solutions. *Nano Lett.* **2009**, *9* (3), 1139−1146.
(97) Baffou, G.; Cichos, F.; Quidant, R. Applications and Challenges of Thermoplasmonics. *Nat. Mater.* **2020**, *19* (9), 946−958.
(98) Chirumamilla, M.; Roberts, A. S.; Ding, F.; Wang, D.; Kristensen, P. K.; Bozhevolnyi, S. I.; Pedersen, K. Multilayer Tungsten-Alumina-Based Broadband Light Absorbers for High-Temperature Applications. *Opt. Mater. Express* **2016**, *6* (8), 2704−2714.
(99) Chen, T.-A.; Un, I.-W.; Wei, C.-C.; Lu, Y.-J.; Tsai, D. P.; Yen, T.-J. Alternating Nanolayers of Dielectric MgF2 and Metallic Ag as Hyperbolic Metamaterials: Probing Surface States and Optical Topological Phase Transition and Implications for Sensing Applications. *ACS Appl. Nano Mater.* **2021**, *4* (2), 2211−2217.
(100) Li, W.; Guler, U.; Kinsey, N.; Naik, G. V.; Boltasseva, A.; Guan, J.; Shalaev, V. M.; Kildishev, A. V. Refractory Plasmonics with Titanium Nitride: Broadband Metamaterial Absorber. *Adv. Mater.* **2014**, *26* (47), 7959−7965.
(101) Ding, F.; Dai, J.; Chen, Y.; Zhu, J.; Jin, Y.; Bozhevolnyi, S. I. Broadband Near-Infrared Metamaterial Absorbers Utilizing Highly Lossy Metals. *Sci. Rep.* **2016**, *6* (1), 39445.
(102) Jahani, S.; Jacob, Z. All-Dielectric Metamaterials. *Nat. Nanotechnol.* **2016**, *11* (1), 23−36.
(103) Castellanos, G. W.; Bai, P.; Gómez Rivas, J. Lattice Resonances in Dielectric Metasurfaces. *J. Appl. Phys.* **2019**, *125* (21), 213105.
(104) Luk'yanchuk, B.; Zheludev, N. I.; Maier, S. A.; Halas, N. J.; Nordlander, P.; Giessen, H.; Chong, C. T. The Fano Resonance in Plasmonic Nanostructures and Metamaterials. *Nat. Mater.* **2010**, *9* (9), 707−715.
(105) Limonov, M. F.; Rybin, M. V.; Poddubny, A. N.; Kivshar, Y. S. Fano Resonances in Photonics. *Nat. Photonics* **2017**, *11* (9), 543−554.
(106) Campione, S.; Guclu, C.; Ragan, R.; Capolino, F. Enhanced Magnetic and Electric Fields via Fano Resonances in Metasurfaces of Circular Clusters of Plasmonic Nanoparticles. *ACS Photonics* **2014**, *1* (3), 254−260.
(107) Liu, Z.; Ye, J. Highly Controllable Double Fano Resonances in Plasmonic Metasurfaces. *Nanoscale* **2016**, *8* (40), 17665−17674.
(108) Shah, Y. D.; Grant, J.; Hao, D.; Kenney, M.; Pusino, V.; Cumming, D. R. S. Ultra-Narrow Line Width Polarization-Insensitive Filter Using a Symmetry-Breaking Selective Plasmonic Metasurface. *ACS Photonics* **2018**, *5* (2), 663−669.
(109) Limonov, M. F. Fano Resonance for Applications. *Adv. Opt. Photonics* **2021**, *13* (3), 703−771.
(110) Campione, S.; Liu, S.; Basilio, L. I.; Warne, L. K.; Langston, W. L.; Luk, T. S.; Wendt, J. R.; Reno, J. L.; Keeler, G. A.; Brener, I.; Sinclair, M. B. Broken Symmetry Dielectric Resonators for High Quality Factor Fano Metasurfaces. *ACS Photonics* **2016**, 3 (12), 2362−2367.
(111) Liu, Y.-C.; Li, B.-B.; Xiao, Y.-F. Electromagnetically Induced Transparency in Optical Microcavities. *Nanophotonics* **2017**, *6* (5), 789−811.
(112) Hsu, C. W.; Zhen, B.; Stone, A. D.; Joannopoulos, J. D.; Soljačić, M. Bound States in the Continuum. *Nat. Rev. Mater.* **2016**, *1* (9), 1−13.
(113) Koshelev, K.; Bogdanov, A.; Kivshar, Y. Meta-Optics and Bound States in the Continuum. *Sci. Bull.* **2019**, *64* (12), 836−842.
(114) Koshelev, K.; Kruk, S.; Melik-Gaykazyan, E.; Choi, J.-H.; Bogdanov, A.; Park, H.-G.; Kivshar, Y. Subwavelength Dielectric Resonators for Nonlinear Nanophotonics. *Science* **2020**, *367* (6475), 288−292.
(115) Zhou, C.; Huang, L.; Jin, R.; Xu, L.; Li, G.; Rahmani, M.; Chen, X.; Lu, W.; Miroshnichenko, A. E. Bound States in the Continuum in Asymmetric Dielectric Metasurfaces. *Laser Photonics Rev.* **2023**, *17* (3), 2200564.
(116) Yang, Y.; Kravchenko, I. I.; Briggs, D. P.; Valentine, J. All-Dielectric Metasurface Analogue of Electromagnetically Induced Transparency. *Nat. Commun.* **2014**, *5* (1), 5753.
(117) Miroshnichenko, A. E.; Evlyukhin, A. B.; Yu, Y. F.; Bakker, R. M.; Chipouline, A.; Kuznetsov, A. I.; Luk'yanchuk, B.; Chichkov, B. N.; Kivshar, Y. S. Nonradiating Anapole Modes in Dielectric Nanoparticles. *Nat. Commun.* **2015**, *6* (1), 8069.
(118) Savinov, V.; Papasimakis, N.; Tsai, D. P.; Zheludev, N. I. Optical Anapoles. *Commun. Phys.* **2019**, *2* (1), 1−4.
(119) Guan, J.; Park, J.-E.; Deng, S.; Tan, M. J. H.; Hu, J.; Odom, T. W. Light-Matter Interactions in Hybrid Material Metasurfaces. *Chem. Rev.* **2022**, *122* (19), 15177−15203.
(120) Wang, F.; Harutyunyan, H. Tailoring the Quality Factors and Nonlinear Response in Hybrid Plasmonic-Dielectric Metasurfaces. *Opt. Express* **2018**, *26* (1), 120−129.

https://doi.org/10.1021/acsphotonics.3c01013
ACS Photonics XXXX, XXX, XXX−XXX

(121) Huang, Y.; Liu, L.; Pu, M.; Li, X.; Ma, X.; Luo, X. A Refractory Metamaterial Absorber for Ultra-Broadband, Omnidirectional and Polarization-Independent Absorption in the UV-NIR Spectrum. *Nanoscale* **2018**, *10* (17), 8298−8303.
(122) Yang, J.; Gurung, S.; Bej, S.; Ni, P.; Howard Lee, H. W. Active Optical Metasurfaces: Comprehensive Review on Physics, Mechanisms, and Prospective Applications. *Rep. Prog. Phys.* **2022**, *85* (3), 036101.
(123) Wang, Q.; Rogers, E. T. F.; Gholipour, B.; Wang, C.-M.; Yuan, G.; Teng, J.; Zheludev, N. I. Optically Reconfigurable Metasurfaces and Photonic Devices Based on Phase Change Materials. *Nat. Photonics* **2016**, *10* (1), 60−65.
(124) Ladutenko, K.; Pal, U.; Rivera, A.; Peña-Rodríguez, O. Mie Calculation of Electromagnetic Near-Field for a Multilayered Sphere. *Comput. Phys. Commun.* **2017**, *214*, 225−230.
(125) Bin-Alam, M. S.; Reshef, O.; Mamchur, Y.; Alam, M. Z.; Carlow, G.; Upham, J.; Sullivan, B. T.; Ménard, J.-M.; Huttunen, M. J.; Boyd, R. W.; Dolgaleva, K. Ultra-High-Q Resonances in Plasmonic Metasurfaces. *Nat. Commun.* **2021**, *12* (1), 974.
(126) Campbell, S. D.; Sell, D.; Jenkins, R. P.; Whiting, E. B.; Fan, J. A.; Werner, D. H. Review of Numerical Optimization Techniques for Meta-Device Design [Invited]. *Opt. Mater. Express* **2019**, *9* (4), 1842.
(127) Minkov, M.; Williamson, I. A. D.; Andreani, L. C.; Gerace, D.; Lou, B.; Song, A. Y.; Hughes, T. W.; Fan, S. Inverse Design of Photonic Crystals through Automatic Differentiation. *ACS Photonics* **2020**, *7* (7), 1729−1741.
(128) Peurifoy, J.; Shen, Y.; Jing, L.; Yang, Y.; Cano-Renteria, F.; DeLacy, B. G.; Joannopoulos, J. D.; Tegmark, M.; Soljačić, M. Nanophotonic Particle Simulation and Inverse Design Using Artificial Neural Networks. *Sci. Adv.* **2018**, *4* (6), No. eaar4206.
(129) Krasikov, S.; Tranter, A.; Bogdanov, A.; Kivshar, Y. Intelligent Metaphotonics Empowered by Machine Learning. *Opto-Electron. Adv.* **2022**, *5* (3), 210147−24.
(130) An, S.; Zheng, B.; Tang, H.; Shalaginov, M. Y.; Zhou, L.; Li, H.; Kang, M.; Richardson, K. A.; Gu, T.; Hu, J.; Fowler, C.; Zhang, H. Multifunctional Metasurface Design with a Generative Adversarial Network. *Adv. Opt. Mater.* **2021**, *9* (5), 2001433.
(131) Ma, W.; Liu, Z.; Kudyshev, Z. A.; Boltasseva, A.; Cai, W.; Liu, Y. Deep Learning for the Design of Photonic Structures. *Nat. Photonics* **2021**, *15* (2), 77−90.
(132) Jiang, J.; Chen, M.; Fan, J. A. Deep Neural Networks for the Evaluation and Design of Photonic Devices. *Nat. Rev. Mater.* **2021**, *6* (8), 679−700.
(133) Yao, K.; Unni, R.; Zheng, Y. Intelligent Nanophotonics: Merging Photonics and Artificial Intelligence at the Nanoscale. *Nanophotonics* **2019**, *8* (3), 339−366.
(134) Fan, J. A. Freeform Metasurface Design Based on Topology Optimization. *MRS Bull.* **2020**, *45* (3), 196−201.
(135) Lin, Z.; Liu, V.; Pestourie, R.; Johnson, S. G. Topology Optimization of Freeform Large-Area Metasurfaces. *Opt. Express* **2019**, *27* (11), 15765.
(136) Wang, E. W.; Sell, D.; Phan, T.; Fan, J. A. Robust Design of Topology-Optimized Metasurfaces. *Opt. Mater. Express* **2019**, *9* (2), 469−482.
(137) Jiang, J.; Fan, J. A. Global Optimization of Dielectric Metasurfaces Using a Physics-Driven Neural Network. *Nano Lett.* **2019**, *19* (8), 5366−5372.
(138) Diaz, A. R.; Sigmund, O. A Topology Optimization Method for Design of Negative Permeability Metamaterials. *Struct. Multidiscip. Optim.* **2010**, *41* (2), 163−177.
(139) Christiansen, R. E.; Sigmund, O. Inverse Design in Photonics by Topology Optimization: Tutorial. *JOSA B* **2021**, *38* (2), 496−509.
(140) Lalau-Keraly, C. M.; Bhargava, S.; Miller, O. D.; Yablonovitch, E. Adjoint Shape Optimization Applied to Electromagnetic Design. *Opt. Express* **2013**, *21* (18), 21693−21701.
(141) Khatib, O.; Ren, S.; Malof, J.; Padilla, W. J. Deep Learning the Electromagnetic Properties of Metamaterials—A Comprehensive Review. *Adv. Funct. Mater.* **2021**, *31* (31), 2101748.
(142) Rycroft, M. J. Computational Electrodynamics, the Finite-Difference Time-Domain Method. *J. Atmospheric Terr. Phys.* **1996**, *58* (15), 1817−1818.
(143) Rumpf, R. C. Simple Implementation of Arbitrarily Shaped Total-Field/Scattered-Field Regions in Finite-Difference Frequency-Domain. *Prog. Electromagn. Res. B* **2012**, *36*, 221−248.
(144) Sumithra, P.; Thiripurasundari, D. Review on Computational Electromagnetics Methods. *Adv. Electromagnetics* **2017**, *6* (1), 42−55.
(145) Christiansen, R. E.; Lin, Z.; Roques-Carmes, C.; Salamin, Y.; Kooi, S. E.; Joannopoulos, J. D.; Soljačić, M.; Johnson, S. G. Fullwave Maxwell Inverse Design of Axisymmetric, Tunable, and Multi-Scale Multi-Wavelength Metalenses. *Opt. Express* **2020**, *28* (23), 33854.
(146) Lin, Z.; Roques-Carmes, C.; Christiansen, R. E.; Soljačić, M.; Johnson, S. G. Computational Inverse Design for Ultra-Compact Single-Piece Metalenses Free of Chromatic and Angular Aberration. *Appl. Phys. Lett.* **2021**, *118* (4), 041104.
(147) Chung, H.; Miller, O. D. High-NA Achromatic Metalenses by Inverse Design. *Opt. Express* **2020**, *28* (5), 6945.
(148) Pestourie, R.; Mroueh, Y.; Nguyen, T. V.; Das, P.; Johnson, S. G. Active Learning of Deep Surrogates for PDEs: Application to Metasurface Design. *Npj Comput. Mater.* **2020**, *6* (1), 164.
(149) Arbabi, E.; Arbabi, A.; Kamali, S. M.; Horie, Y.; Faraon, A. Multiwavelength Polarization-Insensitive Lenses Based on Dielectric Metasurfaces with Meta-Molecules. *Optica* **2016**, *3* (6), 628.
(150) Fan, Z.-B.; Shao, Z.-K.; Xie, M.-Y.; Pang, X.-N.; Ruan, W.-S.; Zhao, F.-L.; Chen, Y.-J.; Yu, S.-Y.; Dong, J.-W. Silicon Nitride Metalenses for Close-to-One Numerical Aperture and Wide-Angle Visible Imaging. *Phys. Rev. Appl.* **2018**, *10* (1), 014005.
(151) Shi, Z.; Khorasaninejad, M.; Huang, Y.-W.; Roques-Carmes, C.; Zhu, A. Y.; Chen, W. T.; Sanjeev, V.; Ding, Z.-W.; Tamagnone, M.; Chaudhary, K.; Devlin, R. C.; Qiu, C.-W.; Capasso, F. Single-Layer Metasurface with Controllable Multiwavelength Functions. *Nano Lett.* **2018**, *18* (4), 2420−2427.
(152) Venter, G. Review of Optimization Techniques. In *Encyclopedia of Aerospace Engineering*; Blockley, R., Shyy, W., Eds.; John Wiley & Sons, Ltd: Chichester, U.K., 2010; p eae495. DOI: 10.1002/9780470686652.eae495.
(153) Lalau-Keraly, C. M.; Bhargava, S.; Miller, O. D.; Yablonovitch, E. Adjoint Shape Optimization Applied to Electromagnetic Design. *Opt. Express* **2013**, *21* (18), 21693.
(154) Bendsøe, M. P.; Sigmund, O. *Topology Optimization*; Springer: Berlin, Heidelberg, 2004. DOI: 10.1007/978-3-662-05086-6.
(155) Jenkins, R. P.; Whiting, E. B.; Campbell, S. D.; Werner, D. H. Improved Convergence in Planar Nanophotonic Topology Optimization via the Multigradient. *Photonics Nanostructures - Fundam. Appl.* **2022**, *52*, 101067.
(156) Yu, S.; Wang, C.; Sun, C.; Chen, W. Topology Optimization for Light-Trapping Structure in Solar Cells. *Struct. Multidiscip. Optim.* **2014**, *50* (3), 367−382.
(157) Park, J.; Kim, S.; Nam, D. W.; Chung, H.; Park, C. Y.; Jang, M. S. Free-Form Optimization of Nanophotonic Devices: From Classical Methods to Deep Learning. *Nanophotonics* **2022**, *11* (9), 1809−1845.
(158) Martí, R. Multi-Start Methods. In *Handbook of Metaheuristics*; Glover, F., Kochenberger, G. A., Eds.; International Series in Operations Research & Management Science; Kluwer Academic Publishers: Boston, 2003; Vol. *57*, pp 355−368. DOI: 10.1007/0-306-48056-5_12.
(159) Floudas, C. A. *Deterministic Global Optimization*; Pardalos, P., Horst, R., Eds.; Nonconvex Optimization and Its Applications; Springer US: Boston, MA, 2000; Vol. *37*. DOI: 10.1007/978-1-4757-4949-6.
(160) Holm, E. A.; Cohn, R.; Gao, N.; Kitahara, A. R.; Matson, T. P.; Lei, B.; Yarasi, S. R. Overview: Computer Vision and Machine Learning for Microstructural Characterization and Analysis. *Metall. Mater. Trans. A* **2020**, *51* (12), 5985−5999.
(161) Nassif, A. B.; Shahin, I.; Attili, I.; Azzeh, M.; Shaalan, K. Speech Recognition Using Deep Neural Networks: A Systematic Review. *IEEE Access* **2019**, *7*, 19143−19165.

https://doi.org/10.1021/acsphotonics.3c01013
ACS Photonics XXXX, XXX, XXX−XXX

(162) Otter, D. W.; Medina, J. R.; Kalita, J. K. A Survey of the Usages of Deep Learning for Natural Language Processing. *IEEE Trans. Neural Netw. Learn. Syst.* **2021**, *32* (2), 604−624.
(163) Kim, D.; Kim, S.-H.; Kim, T.; Kang, B. B.; Lee, M.; Park, W.; Ku, S.; Kim, D.; Kwon, J.; Lee, H.; Bae, J.; Park, Y.-L.; Cho, K.-J.; Jo, S. Review of Machine Learning Methods in Soft Robotics. *PLoS One* **2021**, *16* (2), No. e0246102.
(164) Punia, S. K.; Kumar, M.; Stephan, T.; Deverajan, G. G.; Patan, R. Performance Analysis of Machine Learning Algorithms for Big Data Classification: ML and AI-Based Algorithms for Big Data Analysis. *Int. J. E-Health Med. Commun.* **2021**, *12* (4), 60−75.
(165) Ma, W.; Liu, Z.; Kudyshev, Z. A.; Boltasseva, A.; Cai, W.; Liu, Y. Deep Learning for the Design of Photonic Structures. *Nat. Photonics* **2021**, *15* (2), 77−90.
(166) Malkiel, I.; Mrejen, M.; Nagler, A.; Arieli, U.; Wolf, L.; Suchowski, H. Plasmonic Nanostructure Design and Characterization via Deep Learning. *Light Sci. Appl.* **2018**, *7* (1), 60.
(167) Yesilyurt, O.; Peana, S.; Mkhitaryan, V.; Pagadala, K.; Shalaev, V. M.; Kildishev, A. V.; Boltasseva, A. Fabrication-Conscious Neural Network Based Inverse Design of Single-Material Variable-Index Multilayer Films: *Nanophotonics* **2023**, *12* (5), 993−1006.
(168) Sajedian, I.; Kim, J.; Rho, J. Finding the Optical Properties of Plasmonic Structures by Image Processing Using a Combination of Convolutional Neural Networks and Recurrent Neural Networks. *Microsyst. Nanoeng.* **2019**, *5* (1), 27.
(169) So, S.; Rho, J. Designing Nanophotonic Structures Using Conditional Deep Convolutional Generative Adversarial Networks. *Nanophotonics* **2019**, *8* (7), 1255−1261.
(170) Ma, W.; Liu, Y. A Data-Efficient Self-Supervised Deep Learning Model for Design and Characterization of Nanophotonic Structures. *Sci. China Phys. Mech. Astron.* **2020**, *63* (8), 284212.
(171) Kudyshev, Z. A.; Kildishev, A. V.; Shalaev, V. M.; Boltasseva, A. Machine Learning-Assisted Global Optimization of Photonic Devices. *Nanophotonics* **2020**, *10* (1), 371−383.
(172) Kudyshev, Z. A.; Kildishev, A. V.; Shalaev, V. M.; Boltasseva, A. Machine-Learning-Assisted Metasurface Design for High-Efficiency Thermal Emitter Optimization. *Appl. Phys. Rev.* **2020**, *7* (2), 021407.
(173) Xu, D.; Luo, Y.; Luo, J.; Pu, M.; Zhang, Y.; Ha, Y.; Luo, X. Efficient Design of a Dielectric Metasurface with Transfer Learning and Genetic Algorithm. *Opt. Mater. Express* **2021**, *11* (7), 1852.
(174) Zhu, R.; Qiu, T.; Wang, J.; Sui, S.; Li, Y.; Feng, M.; Ma, H.; Qu, S. Multiplexing the Aperture of a Metasurface: Inverse Design via Deep-Learning-Forward Genetic Algorithm. *J. Phys. Appl. Phys.* **2020**, *53* (45), 455002.
(175) Elsawy, M. M. R.; Lanteri, S.; Duvigneau, R.; Brière, G.; Mohamed, M. S.; Genevet, P. Global Optimization of Metasurface Designs Using Statistical Learning Methods. *Sci. Rep.* **2019**, *9* (1), 17918.
(176) Elsawy, M. M. R.; Lanteri, S.; Duvigneau, R.; Fan, J. A.; Genevet, P. Numerical Optimization Methods for Metasurfaces. *Laser Photonics Rev.* **2020**, *14* (10), 1900445.
(177) Jiang, J.; Sell, D.; Hoyer, S.; Hickey, J.; Yang, J.; Fan, J. A. Free-Form Diffractive Metagrating Design Based on Generative Adversarial Networks. *ACS Nano* **2019**, *13* (8), 8872−8878.
(178) Sullivan, J.; Mirhashemi, A.; Lee, J. Deep Learning Based Analysis of Microstructured Materials for Thermal Radiation Control. *Sci. Rep.* **2022**, *12* (1), 9785.
(179) Du, X.; Zhou, C.; Bai, H.; Liu, X. Inverse Design Paradigm for Fast and Accurate Prediction of a Functional Metasurface via Deep Convolutional Neural Networks. *Opt. Mater. Express* **2022**, *12* (10), 4104.
(180) So, S.; Yang, Y.; Lee, T.; Rho, J. On-Demand Design of Spectrally Sensitive Multiband Absorbers Using an Artificial Neural Network. *Photonics Res.* **2021**, *9* (4), B153.
(181) Ding, W.; Chen, J.; Wu, R.-x. A Generative Meta-Atom Model for Metasurface-Based Absorber Designs. *Adv. Opt. Mater.* **2023**, *11*, 2201959.
(182) Deng, Y.; Ren, S.; Malof, J.; Padilla, W. J. Deep Inverse Photonic Design: A Tutorial. *Photonics Nanostructures - Fundam. Appl.* **2022**, *52*, 101070.
(183) Aryal, U. K.; Ahmadpour, M.; Turkovic, V.; Rubahn, H.-G.; Di Carlo, A.; Madsen, M. 2D Materials for Organic and Perovskite Photovoltaics. *Nano Energy* **2022**, *94*, 106833.
(184) Günes, S.; Neugebauer, H.; Sariciftci, N. S. Conjugated Polymer-Based Organic Solar Cells. *Chem. Rev.* **2007**, *107* (4), 1324−1338.
(185) Atwater, H. A.; Polman, A. Plasmonics for Improved Photovoltaic Devices. *Nat. Mater.* **2010**, *9* (3), 205−213.
(186) Elshorbagy, M. H.; Sánchez, P. A.; Cuadrado, A.; Alda, J.; Esteban, Ó. Resonant Nano-Dimer Metasurface for Ultra-Thin a-Si:H Solar Cells. *Sci. Rep.* **2021**, *11* (1), 7179.
(187) Pala, R. A.; Butun, S.; Aydin, K.; Atwater, H. A. Omnidirectional and Broadband Absorption Enhancement from Trapezoidal Mie Resonators in Semiconductor Metasurfaces. *Sci. Rep.* **2016**, *6* (1), 31451.
(188) Odebo Länk, N.; Verre, R.; Johansson, P.; Käll, M. Large-Scale Silicon Nanophotonic Metasurfaces with Polarization Independent Near-Perfect Absorption. *Nano Lett.* **2017**, *17* (5), 3054−3060.
(189) Esfandyarpour, M.; Garnett, E. C.; Cui, Y.; McGehee, M. D.; Brongersma, M. L. Metamaterial Mirrors in Optoelectronic Devices. *Nat. Nanotechnol.* **2014**, *9* (7), 542−547.
(190) Ou, Q.-D.; Xie, H.-J.; Chen, J.-D.; Zhou, L.; Li, Y.-Q.; Tang, J.-X. Enhanced Light Harvesting in Flexible Polymer Solar Cells: Synergistic Simulation of a Plasmonic Meta-Mirror and a Transparent Silver Mesowire Electrode. *J. Mater. Chem. A* **2016**, *4* (48), 18952−18962.
(191) Shameli, M. A.; Yousefi, L. Absorption Enhancement in Thin-Film Solar Cells Using an Integrated Metasurface Lens. *JOSA B* **2018**, *35* (2), 223−230.
(192) Cai, J.; Qi, L. Recent Advances in Antireflective Surfaces Based on Nanostructure Arrays. *Mater. Horiz.* **2015**, *2* (1), 37−53.
(193) Spinelli, P.; Verschuuren, M. A.; Polman, A. Broadband Omnidirectional Antireflection Coating Based on Subwavelength Surface Mie Resonators. *Nat. Commun.* **2012**, *3* (1), 692.
(194) Pecora, E. F.; Cordaro, A.; Kik, P. G.; Brongersma, M. L. Broadband Antireflection Coatings Employing Multiresonant Dielectric Metasurfaces. *ACS Photonics* **2018**, *5* (11), 4456−4462.
(195) Piechulla, P. M.; Slivina, E.; Bätzner, D.; Fernandez-Corbaton, I.; Dhawan, P.; Wehrspohn, R. B.; Sprafke, A. N.; Rockstuhl, C. Antireflective Huygens' Metasurface with Correlated Disorder Made from High-Index Disks Implemented into Silicon Heterojunction Solar Cells. *ACS Photonics* **2021**, *8* (12), 3476−3485.
(196) Uleman, F.; Neder, V.; Cordaro, A.; Alù, A.; Polman, A. Resonant Metagratings for Spectral and Angular Control of Light for Colored Rooftop Photovoltaics. *ACS Appl. Energy Mater.* **2020**, *3* (4), 3150−3156.
(197) Ferry, V. E.; Sweatlock, L. A.; Pacifici, D.; Atwater, H. A. Plasmonic Nanostructure Design for Efficient Light Coupling into Solar Cells. *Nano Lett.* **2008**, *8* (12), 4391−4397.
(198) Simovski, C.; Morits, D.; Voroshilov, P.; Guzhva, M.; Belov, P.; Kivshar, Y. Enhanced Efficiency of Light-Trapping Nanoantenna Arrays for Thin-Film Solar Cells. *Opt. Express* **2013**, *21* (104), A714−A725.
(199) Voroshilov, P. M.; Ovchinnikov, V.; Papadimitratos, A.; Zakhidov, A. A.; Simovski, C. R. Light Trapping Enhancement by Silver Nanoantennas in Organic Solar Cells. *ACS Photonics* **2018**, *5* (5), 1767−1772.
(200) Chen, X.; Shen, S.; Guo, L.; Mao, S. S. Semiconductor-Based Photocatalytic Hydrogen Generation. *Chem. Rev.* **2010**, *110* (11), 6503−6570.
(201) Ghobadi, A.; Ulusoy Ghobadi, T. G.; Karadas, F.; Ozbay, E. Semiconductor Thin Film Based Metasurfaces and Metamaterials for Photovoltaic and Photoelectrochemical Water Splitting Applications. *Adv. Opt. Mater.* **2019**, *7* (14), 1900028.
(202) Nwosu, U.; Wang, A.; Palma, B.; Zhao, H.; Khan, M. A.; Kibria, M.; Hu, J. Selective Biomass Photoreforming for Valuable Chemicals

https://doi.org/10.1021/acsphotonics.3c01013
ACS Photonics XXXX, XXX, XXX−XXX

and Fuels: A Critical Review. *Renew. Sustain. Energy Rev.* **2021**, *148*, 111266.
(203) Ma, J.; Liu, K.; Yang, X.; Jin, D.; Li, Y.; Jiao, G.; Zhou, J.; Sun, R. Recent Advances and Challenges in Photoreforming of Biomass-Derived Feedstocks into Hydrogen, Biofuels, or Chemicals by Using Functional Carbon Nitride Photocatalysts. *ChemSusChem* **2021**, *14* (22), 4903−4922.
(204) Bosomtwi, D.; Osiński, M.; Babicheva, V. E. Lattice Effect for Enhanced Hot-Electron Generation in Nanoelectrodes. *Opt. Mater. Express* **2021**, *11* (9), 3232−3244.
(205) Deng, S.; Zhang, B.; Choo, P.; Smeets, P. J. M.; Odom, T. W. Plasmonic Photoelectrocatalysis in Copper-Platinum Core-Shell Nanoparticle Lattices. *Nano Lett.* **2021**, *21* (3), 1523−1529.
(206) Xu, R.; Wen, L.; Wang, Z.; Zhao, H.; Mu, G.; Zeng, Z.; Zhou, M.; Bohm, S.; Zhang, H.; Wu, Y.; Runge, E.; Lei, Y. Programmable Multiple Plasmonic Resonances of Nanoparticle Superlattice for Enhancing Photoelectrochemical Activity. *Adv. Funct. Mater.* **2020**, *30* (48), 2005170.
(207) Li, J.; Cushing, S. K.; Zheng, P.; Meng, F.; Chu, D.; Wu, N. Plasmon-Induced Photonic and Energy-Transfer Enhancement of Solar Water Splitting by a Hematite Nanorod Array. *Nat. Commun.* **2013**, *4* (1), 2651.
(208) Yalavarthi, R.; Yesilyurt, O.; Henrotte, O.; Kment, Š.; Shalaev, V. M.; Boltasseva, A.; Naldoni, A. Multimetallic Metasurfaces for Enhanced Electrocatalytic Oxidations in Direct Alcohol Fuel Cells. *Laser Photonics Rev.* **2022**, *16* (7), 2200137.
(209) Yalavarthi, R.; Henrotte, O.; Kment, Š.; Naldoni, A. Determining the Role of Pd Catalyst Morphology and Deposition Criteria over Large Area Plasmonic Metasurfaces during Light-Enhanced Electrochemical Oxidation of Formic Acid. *J. Chem. Phys.* **2022**, *157* (11), 114706.
(210) Wu, Y.; Yang, W.; Fan, Y.; Song, Q.; Xiao, S. TiO2Metasurfaces: From Visible Planar Photonics to Photochemistry. *Sci. Adv.* **2019**, *5* (11), No. eaax0939.
(211) Hu, H.; Weber, T.; Bienek, O.; Wester, A.; Hüttenhofer, L.; Sharp, I. D.; Maier, S. A.; Tittl, A.; Cortés, E. Catalytic Metasurfaces Empowered by Bound States in the Continuum. *ACS Nano* **2022**, *16* (8), 13057−13068.
(212) Xiao, Q.; Connell, T. U.; Cadusch, J. J.; Roberts, A.; Chesman, A. S. R.; Gómez, D. E. Hot-Carrier Organic Synthesis via the Near-Perfect Absorption of Light. *ACS Catal.* **2018**, *8* (11), 10331−10339.
(213) Wang, W.; Besteiro, L. V.; Liu, T.; Wu, C.; Sun, J.; Yu, P.; Chang, L.; Wang, Z.; Govorov, A. O. Generation of Hot Electrons with Chiral Metamaterial Perfect Absorbers: Giant Optical Chirality for Polarization-Sensitive Photochemistry. *ACS Photonics* **2019**, *6* (12), 3241−3252.
(214) Wei, X.; Liu, J.; Xia, G.-J.; Deng, J.; Sun, P.; Chruma, J. J.; Wu, W.; Yang, C.; Wang, Y.-G.; Huang, Z. Enantioselective Photoinduced Cyclodimerization of a Prochiral Anthracene Derivative Adsorbed on Helical Metal Nanostructures. *Nat. Chem.* **2020**, *12* (6), 551−559.
(215) Xiao, Q.; Kinnear, C.; Connell, T. U.; Kashif, M. K.; Easton, C. D.; Seeber, A.; Bourgeois, L.; Bonin, Gus. O.; Duffy, N. W.; Chesman, A. S. R.; Gómez, D. E. Dual Photolytic Pathways in an Alloyed Plasmonic Near-Perfect Absorber: Implications for Photoelectrocatalysis. *ACS Appl. Nano Mater.* **2021**, *4* (3), 2702−2712.
(216) Baranov, D. G.; Zuev, D. A.; Lepeshov, S. I.; Kotov, O. V.; Krasnok, A. E.; Evlyukhin, A. B.; Chichkov, B. N. All-Dielectric Nanophotonics: The Quest for Better Materials and Fabrication Techniques. *Optica* **2017**, *4* (7), 814−825.
(217) Naldoni, A.; Guler, U.; Wang, Z.; Marelli, M.; Malara, F.; Meng, X.; Besteiro, L. V.; Govorov, A. O.; Kildishev, A. V.; Boltasseva, A.; Shalaev, V. M. Broadband Hot-Electron Collection for Solar Water Splitting with Plasmonic Titanium Nitride. *Adv. Opt. Mater.* **2017**, *5* (15), 1601031.
(218) Xu, L.; Rahmani, M.; Ma, Y.; Smirnova, D. A.; Kamali, K. Z.; Deng, F.; Chiang, Y. K.; Huang, L.; Zhang, H.; Gould, S.; Neshev, D. N.; Miroshnichenko, A. E. Enhanced Light-Matter Interactions in Dielectric Nanostructures via Machine-Learning Approach. *Adv. Photonics* **2020**, *2* (2), 026003.
(219) Ma, W.; Xu, Y.; Xiong, B.; Deng, L.; Peng, R.-W.; Wang, M.; Liu, Y. Pushing the Limits of Functionality-Multiplexing Capability in Metasurface Design Based on Statistical Machine Learning. *Adv. Mater.* **2022**, *34* (16), 2110022.
(220) Neumann, O.; Neumann, A. D.; Tian, S.; Thibodeaux, C.; Shubhankar, S.; Müller, J.; Silva, E.; Alabastri, A.; Bishnoi, S. W.; Nordlander, P.; Halas, N. J. Combining Solar Steam Processing and Solar Distillation for Fully Off-Grid Production of Cellulosic Bioethanol. *ACS Energy Lett.* **2017**, *2* (1), 8−13.
(221) Dongare, P. D.; Alabastri, A.; Pedersen, S.; Zodrow, K. R.; Hogan, N. J.; Neumann, O.; Wu, J.; Wang, T.; Deshmukh, A.; Elimelech, M.; Li, Q.; Nordlander, P.; Halas, N. J. Nanophotonics-Enabled Solar Membrane Distillation for off-Grid Water Purification. *Proc. Natl. Acad. Sci. U. S. A.* **2017**, *114* (27), 6936−6941.
(222) Schmid, W.; Machorro-Ortiz, A.; Jerome, B.; Naldoni, A.; Halas, N. J.; Dongare, P. D.; Alabastri, A. Decentralized Solar-Driven Photothermal Desalination: An Interdisciplinary Challenge to Transition Lab-Scale Research to Off-Grid Applications. *ACS Photonics* **2022**, *9* (12), 3764−3776.
(223) Zhou, L.; Tan, Y.; Wang, J.; Xu, W.; Yuan, Y.; Cai, W.; Zhu, S.; Zhu, J. 3D Self-Assembly of Aluminium Nanoparticles for Plasmon-Enhanced Solar Desalination. *Nat. Photonics* **2016**, *10* (6), 393−398.
(224) Zhou, L.; Tan, Y.; Ji, D.; Zhu, B.; Zhang, P.; Xu, J.; Gan, Q.; Yu, Z.; Zhu, J. Self-Assembly of Highly Efficient, Broadband Plasmonic Absorbers for Solar Steam Generation. *Sci. Adv.* **2016**, *2* (4), No. e1501227.
(225) Kaur, M.; Ishii, S.; Shinde, S. L.; Nagao, T. All-Ceramic Solar-Driven Water Purifier Based on Anodized Aluminum Oxide and Plasmonic Titanium Nitride. *Adv. Sustain. Syst.* **2019**, *3* (2), 1800112.
(226) Liu, Y.; Song, H.; Bei, Z.; Zhou, L.; Zhao, C.; Ooi, B. S.; Gan, Q. Ultra-Thin Dark Amorphous TiOx Hollow Nanotubes for Full Spectrum Solar Energy Harvesting and Conversion‡. *Nano Energy* **2021**, *84*, 105872.
(227) Mascaretti, L.; Schirato, A.; Zbořil, R.; Kment, Š.; Schmuki, P.; Alabastri, A.; Naldoni, A. Solar Steam Generation on Scalable Ultrathin Thermoplasmonic TiN Nanocavity Arrays. *Nano Energy* **2021**, *83*, 105828.
(228) Chen, W.; Gao, Y.; Li, Y.; Yan, Y.; Ou, J.-Y.; Ma, W.; Zhu, J. Broadband Solar Metamaterial Absorbers Empowered by Transformer-Based Deep Learning. *Adv. Sci.* **2023**, *10* (13), 2206718.
(229) Chang, C.-C.; Kort-Kamp, W. J. M.; Nogan, J.; Luk, T. S.; Azad, A. K.; Taylor, A. J.; Dalvit, D. A. R.; Sykora, M.; Chen, H.-T. High-Temperature Refractory Metasurfaces for Solar Thermophotovoltaic Energy Harvesting. *Nano Lett.* **2018**, *18* (12), 7665−7673.
(230) Rinnerbauer, V.; Lenert, A.; Bierman, D. M.; Yeng, Y. X.; Chan, W. R.; Geil, R. D.; Senkevich, J. J.; Joannopoulos, J. D.; Wang, E. N.; Soljačić, M.; Celanovic, I. Metallic Photonic Crystal Absorber-Emitter for Efficient Spectral Control in High-Temperature Solar Thermophotovoltaics. *Adv. Energy Mater.* **2014**, *4* (12), 1400334.
(231) Rana, A. S.; Zubair, M.; Chen, Y.; Wang, Z.; Deng, J.; Chani, M. T. S.; Danner, A.; Teng, J.; Mehmood, M. Q. Broadband Solar Absorption by Chromium Metasurface for Highly Efficient Solar Thermophotovoltaic Systems. *Renew. Sustain. Energy Rev.* **2023**, *171*, 113005.
(232) Chirumamilla, M.; Chirumamilla, A.; Yang, Y.; Roberts, A. S.; Kristensen, P. K.; Chaudhuri, K.; Boltasseva, A.; Sutherland, D. S.; Bozhevolnyi, S. I.; Pedersen, K. Large-Area Ultrabroadband Absorber for Solar Thermophotovoltaics Based on 3D Titanium Nitride Nanopillars. *Adv. Opt. Mater.* **2017**, *5* (22), 1700552.
(233) Chou, J. B.; Yeng, Y. X.; Lee, Y. E.; Lenert, A.; Rinnerbauer, V.; Celanovic, I.; Soljačić, M.; Fang, N. X.; Wang, E. N.; Kim, S.-G. Enabling Ideal Selective Solar Absorption with 2D Metallic Dielectric Photonic Crystals. *Adv. Mater.* **2014**, *26* (47), 8041−8045.
(234) Zhang, F.; Li, Y.-H.; Qi, M.-Y.; Yamada, Y. M. A.; Anpo, M.; Tang, Z.-R.; Xu, Y.-J. Photothermal Catalytic CO2 Reduction over Nanomaterials. *Chem. Catal.* **2021**, *1* (2), 272−297.
(235) Naldoni, A.; Kudyshev, Z. A.; Mascaretti, L.; Sarmah, S. P.; Rej, S.; Froning, J. P.; Tomanec, O.; Yoo, J. E.; Wang, D.; Kment, Š.; Montini, T.; Fornasiero, P.; Shalaev, V. M.; Schmuki, P.; Boltasseva, A.;

https://doi.org/10.1021/acsphotonics.3c01013
ACS Photonics XXXX, XXX, XXX−XXX

Zbořil, R. Solar Thermoplasmonic Nanofurnace for High-Temperature Heterogeneous Catalysis. *Nano Lett.* **2020**, *20* (5), 3663−3672.
(236) Nguyen, N. T.; Xia, M.; Duchesne, P. N.; Wang, L.; Mao, C.; Ali, F. M.; Yan, T.; Li, P.; Lu, Z.-H.; Ozin, G. A. Enhanced CO2 Photocatalysis by Indium Oxide Hydroxide Supported on TiN@TiO_2 Nanotubes. *Nano Lett.* **2021**, *21* (3), 1311−1319.
(237) Hong, J.; Xu, C.; Deng, B.; Gao, Y.; Zhu, X.; Zhang, X.; Zhang, Y. Photothermal Chemistry Based on Solar Energy: From Synergistic Effects to Practical Applications. *Adv. Sci.* **2022**, *9* (3), 2103926.
(238) Gao, W.; Chen, Y. Emerging Materials and Strategies for Passive Daytime Radiative Cooling. *Small* **2023**, *19* (18), 2206145.
(239) Rephaeli, E.; Raman, A.; Fan, S. Ultrabroadband Photonic Structures To Achieve High-Performance Daytime Radiative Cooling. *Nano Lett.* **2013**, *13* (4), 1457−1461.
(240) Li, W.; Shi, Y.; Chen, K.; Zhu, L.; Fan, S. A Comprehensive Photonic Approach for Solar Cell Cooling. *ACS Photonics* **2017**, *4* (4), 774−782.
(241) Zhu, L.; Raman, A. P.; Fan, S. Radiative Cooling of Solar Absorbers Using a Visibly Transparent Photonic Crystal Thermal Blackbody. *Proc. Natl. Acad. Sci. U. S. A.* **2015**, *112* (40), 12282−12287.
(242) Hossain, M. M.; Jia, B.; Gu, M. A Metamaterial Emitter for Highly Efficient Radiative Cooling. *Adv. Opt. Mater.* **2015**, *3* (8), 1047−1051.
(243) Cho, J.-W.; Park, S.-J.; Park, S.-J.; Kim, Y.-B.; Moon, Y.-J.; Kim, S.-K. Cooling Metals via Gap Plasmon Resonance. *Nano Lett.* **2021**, *21* (9), 3974−3980.
(244) Zou, C.; Ren, G.; Hossain, M. M.; Nirantar, S.; Withayachumnankul, W.; Ahmed, T.; Bhaskaran, M.; Sriram, S.; Gu, M.; Fumeaux, C. Metal-Loaded Dielectric Resonator Metasurfaces for Radiative Cooling. *Adv. Opt. Mater.* **2017**, *5* (20), 1700460.
(245) Dang, S.; Wang, X.; Ye, H. An Ultrathin Transparent Radiative Cooling Photonic Structure with a High NIR Reflection. *Adv. Mater. Interfaces* **2022**, *9* (30), 2201050.
(246) Long, L.; Taylor, S.; Wang, L. Enhanced Infrared Emission by Thermally Switching the Excitation of Magnetic Polariton with Scalable Microstructured VO2Metasurfaces. *ACS Photonics* **2020**, *7* (8), 2219−2227.
(247) Sun, K.; Xiao, W.; Wheeler, C.; Simeoni, M.; Urbani, A.; Gaspari, M.; Mengali, S.; de Groot, C. H. K.; Muskens, O. L. VO2Metasurface Smart Thermal Emitter with High Visual Transparency for Passive Radiative Cooling Regulation in Space and Terrestrial Applications. *Nanophotonics* **2022**, *11* (17), 4101−4114.
(248) Wang, W.; Zhao, Z.; Zou, Q.; Hong, B.; Zhang, W.; Wang, G. P. Self-Adaptive Radiative Cooling and Solar Heating Based on a Compound Metasurface. *J. Mater. Chem. C* **2020**, *8* (9), 3192−3199.

https://doi.org/10.1021/acsphotonics.3c01013
ACS Photonics XXXX, XXX, XXX−XXX